# Renormalization of quark propagator, vertex functions, and twist-2 operators from twisted-mass lattice QCD at $N_f = 4$

Benoît Blossier,[1] Mariane Brinet,[2] Pierre Guichon,[3] Vincent Morénas,[4] Olivier Pène,[1] Jose Rodríguez-Quintero,[5] and Savvas Zafeiropoulos[4,6]

[1]*Laboratoire de Physique Théorique—CNRS et Université Paris-Sud XI, Bâtiment 210, 91405 Orsay Cedex, France*

[2]*Laboratoire de Physique Subatomique et de Cosmologie—Université Grenoble-Alpes, CNRS/IN2P3, 53, avenue des Martyrs, 38026 Grenoble, France*

[3]*CEA-Saclay, IRFU/SPhN, 91191 Gif-sur-Yvette, France*

[4]*Laboratoire de Physique Corpusculaire—Université Blaise Pascal, CNRS/IN2P3, 63000 Aubière Cedex, France*

[5]*Departamento Física Aplicada—Facultad de Ciencias Experimentales, Universidad de Huelva, 21071 Huelva, Spain*

[6]*Institut für Theoretische Physik, Goethe-Universität Frankfurt, Max-von-Laue-Straße 1, 60438 Frankfurt am Main, Germany*

(Received 3 November 2014; published 24 June 2015)

We present a precise nonperturbative determination of the renormalization constants in the mass independent RI'-MOM scheme. The lattice implementation uses the Iwasaki gauge action and four degenerate dynamical twisted-mass fermions. The gauge configurations are provided by the ETM Collaboration. Renormalization constants for scalar, pseudoscalar, vector and axial operators, as well as the quark propagator renormalization, are computed at three different values of the lattice spacing, two volumes and several twisted-mass parameters. The method we developed allows for a precise cross-check of the running, thanks to the particular proper treatment of hypercubic artifacts. Results for the twist-2 operator $O_{44}$ are also presented.

DOI: 10.1103/PhysRevD.91.114507 PACS numbers: 11.15.Ha, 03.70.+k, 11.10.Gh, 11.15.-q

## I. INTRODUCTION

Lattice QCD (LQCD) has proven to be a very powerful approach to study QCD and has become a precision technique for the *ab initio* computation of many QCD observables. In particular, the possibility to perform a rigorous nonperturbative renormalization is an essential feature of lattice calculations. QCD discretization on a space-time lattice provides indeed a well-defined regularization of the theory, by introducing the lattice spacing as a natural cutoff. However, any comparison with physical results requires a precise control of the continuum limit. Renormalization allows us, from bare quantities computed at finite lattice spacing, to obtain meaningful physical observables with the accuracy sought (typically of the percent level). Controlling as much as possible all statistical and systematic effects in the determination of the renormalization constants is crucial since the accuracy of the renormalization procedure directly affects the precision of the computed observables. For instance, the calculation of nucleon matrix elements, which remains an open challenge, involves a careful estimate of the corresponding renormalization constants, essential to compare lattice results to values deduced from experiments. A proper comparison of these matrix elements with experimental values represents both a challenge and an opportunity for lattice QCD.

The goal of this work is to present the computation of renormalization constants (RCs) for local and twist-2 fermionic bilinear operators using twisted-mass fermion configurations with four dynamical quarks in the sea.

We use a modified version of the regularization invariant RI-MOM scheme known as RI'-MOM [1]. The renormalization conditions of an operator are imposed nonperturbatively on conveniently defined amputated projected Green functions computed between off-shell quark states, evaluated at a given momentum and in a fixed gauge. This scheme is mass independent and renormalization constants are defined at zero quark mass. To carry out this renormalization study, the European Twisted Mass Collaboration (ETMC) has performed dedicated $N_f = 4$ simulations with four degenerate light quark masses. RCs for $N_f = 2 + 1 + 1$ ensembles are evaluated by extrapolating to the chiral limit the RCs computed with the $N_f = 4$ ensembles.

By using the lattice formalism, one is obliged to break some symmetries which are only recovered in the continuum limit, among which is the continuum rotation symmetry. In discrete Euclidean space, the $O(4)$ rotation symmetry is broken down to $H(4)$ or $H(3)$ hypercubic symmetry depending on whether the lattice setup is the same on spatial and temporal directions. As a consequence, there are lattice artifacts which are only invariant under $H(4)$ but not

 

under $O(4)$. This is particularly an issue for the computation of quantities like the renormalization constants since the associated statistical errors are often quite small, and the uncertainties from lattice artifacts become visible, thus deserving a careful treatment. A popular solution is to use the "democratic cuts" to select data points with relatively small $H(4)$ lattice artifacts. Another approach, which is usually called the $H(4)$-extrapolation [2–4], is to include the lattice artifacts explicitly in the data analysis. This approach, applied in the present work, allows one to use a much wider range of data points and to extract information from the lattice simulations more efficiently.

A particularly interesting point of the $H(4)$-extrapolation procedure applied to the determination of renormalization constants, is to allow a precise study of their running. This key advantage provides the possibility to compare the evolution of the RCs obtained on the lattice with perturbative formulas and to perform an interesting estimate of the nonperturbative contributions.

This paper is organized as follows. After a brief description of the lattice setup in Sec. II, basic RI'-MOM formulas and our notation are defined in Sec. III. The analysis procedure is explained in Sec. IV, where Goldstone pole subtraction, $m_{PCAC}$ average and hypercubic corrections are detailed. A precise study of the running is presented in Sec. V, both for local and twist-2 operators, with a special focus on lattice artifacts and higher order corrections. A comment is in order at this point. In the jargon of the renormalization community there is an abuse of the meaning of the word "local." All operators considered in this analysis such as densities, currents as well as twist-2 operators are of course local from the field theoretical viewpoint. However, it has prevailed within the renormalization community to refer to local operators in particular for the densities and the currents. Chiral extrapolations are performed in Sec. VI and Sec. VII presents in detail the way we convert our results to the $\overline{\text{MS}}$ scheme. In the penultimate section, Sec. VIII, we estimate the systematic errors and the final section contains our conclusions. It is noteworthy that our methods allow for the extraction of the $\langle A^2 \rangle$, the Landau gauge dimension-2 gluon condensate [5] that has rich phenomenological implications [6].

## II. LATTICE SETUP

The results presented here are based on the gauge field configurations generated by the ETMC using the Iwasaki gauge action and the twisted-mass fermionic action. Since the RI'-MOM is a mass-independent scheme, where the renormalization conditions are imposed on the chiral limit, the ETMC has generated dedicated $N_f = 4$ ensembles with four light degenerate quarks [7,8], which would eventually allow for a more trustworthy chiral extrapolation. This is the reason we employ these configurations in our analysis, since the physical configurations with two light degenerate $u$ and $d$ quarks and two heavier nondegenerate $s$ and $c$ quarks would introduce an extra source of rather uncontrolled systematic uncertainty. Of course the results obtained with our configurations are intended to renormalize bare matrix elements which are computed with the physical configurations. To achieve automatic $\mathcal{O}(a)$ improvement, the twisted mass action is usually tuned to maximal twist, by tuning $m_{PCAC}$ quark mass to zero. However, in the case of four degenerate quarks, reaching the maximal twist is far from being a trivial task and an alternative option has been chosen. Ensembles are simulated in pairs, with opposite values of $m_{PCAC}$, and $\mathcal{O}(a)$ artifacts are removed by averaging the quantities obtained from these two ensembles. Previous studies have indeed shown the feasibility of this approach [7,9,10]. We refer to Refs. [7,8] for more explicit details and for the original discussion of the computational setup. However, for the sake of completion we will remind the reader all the essential aspects of the algorithmic details as well as the parameter tuning of the ensemble generation. More specifically, the full action reads

$$\mathcal{S}^{(N_f=4)} = \mathcal{S}_g[U] + \mathcal{S}^{\text{sea}}_{TM}[\chi^{\text{sea}}_f, U] + \mathcal{S}^{\text{val}}_{TM}[\chi_f, \phi_f, U], \tag{1}$$

where by $\chi$ we denote the usual "fermionic" quarks both in the sea and the valence sector and by $\phi$ the "bosonic" quarks used in the partial quenching. The fermionic action for the sea quarks takes the form

$$S^{\text{sea}}_{tm} = a^4 \sum_{x,f} \bar{\chi}^{\text{sea}}_f [\gamma \cdot \tilde{\nabla} + W_{cr} + (m^{\text{sea}}_{0f} - m_{cr}) + i r^{\text{sea}}_f \mu^{\text{sea}}_f \gamma_5] \chi^{\text{sea}}_f, \tag{2}$$

with $\gamma \cdot \tilde{\nabla} = \frac{\gamma_\mu}{2}(\nabla_\mu + \nabla^*_\mu)$, $W_{cr} = -\frac{a}{2}\nabla^*_\mu \nabla_\mu + m_{cr}$ and $r^{\text{sea}}_d = -r^{\text{sea}}_u$, $r^{\text{sea}}_c = -r^{\text{sea}}_s$. For the twisted-mass parameter the following choice has been made:

$$\mu^{\text{sea}}_u = \mu^{\text{sea}}_d = \mu^{\text{sea}}_s = \mu^{\text{sea}}_c \equiv \mu^{\text{sea}}. \tag{3}$$

Accordingly, the fermionic action for the valence quarks takes the form

$$S^{\text{val}} = a^4 \sum_{x,f} \bar{\chi}^{\text{val}}_f [\gamma \cdot \tilde{\nabla} - \frac{a}{2}\nabla^*_\mu \nabla_\mu + m^{\text{val}}_{0,f} + i r^{\text{val}}_f \mu^{\text{val}}_f \gamma_5] \chi^{\text{val}}_f. \tag{4}$$

The parameters $r^{\text{val/sea}}_f$ take the values $\pm 1$, while the twisted masses $a\mu^{\text{val,sea}}_f$ are assumed to be non-negative. Two volumes, three values of the lattice spacing, and several values of the twisted mass have been considered in the analysis. The run parameters are summarized in Table I

TABLE I. $N_f = 4$ ensembles used in our analysis.

| Ensemble | $\kappa$ | $am_{PCAC}$ | $a\mu$ ($a\mu_{\rm sea}$ in bold) | Configurations |
|---|---|---|---|---|
| | | | $\beta = 2.10$ & $V/a^4 = 32^3 \times 64$ | |
| 3p | 0.156017 | +0.00559(14) | 0.0025, **0.0046**, 0.0090, 0.0152, 0.0201, 0.0249, 0.0297 | 250 |
| 3m | 0.156209 | −0.00585(08) | 0.0025, **0.0046**, 0.0090, 0.0152, 0.0201, 0.0249, 0.0297 | 250 |
| 4p | 0.155983 | +0.00685(12) | 0.0039, **0.0064**, 0.0112, 0.0184, 0.0240, 0.0295 | 210 |
| 4m | 0.156250 | −0.00682(13) | 0.0039, **0.0064**, 0.0112, 0.0184, 0.0240, 0.0295 | 210 |
| 5p | 0.155949 | +0.00823(08) | 0.0048, **0.0078**, 0.0119, 0.0190, 0.0242, 0.0293 | 220 |
| 5m | 0.156291 | −0.00821(11) | 0.0048, **0.0078**, 0.0119, 0.0190, 0.0242, 0.0293 | 220 |
| | | | $\beta = 1.95$ & $V/a^4 = 24^3 \times 48$ | |
| 2p | 0.160826 | +0.01906(24) | **0.0085**, 0.0150, 0.0203, 0.0252, 0.0298 | 290 |
| 2m | 0.161229 | −0.02091(16) | **0.0085**, 0.0150, 0.0203, 0.0252, 0.0298 | 290 |
| 3p | 0.160826 | +0.01632(21) | 0.0060, 0.0085, 0.0120, 0.0150, **0.0180**, 0.0203, 0.0252, 0.0298 | 310 |
| 3m | 0.161229 | −0.01602(20) | 0.0060, 0.0085, 0.0120, 0.0150, **0.0180**, 0.0203, 0.0252, 0.0298 | 310 |
| 8p | 0.160524 | +0.03634(14) | **0.0020**, 0.0085, 0.0150, 0.0203, 0.0252, 0.0298 | 310 |
| 8m | 0.161585 | −0.03627(11) | **0.0020**, 0.0085, 0.0150, 0.0203, 0.0252, 0.0298 | 310 |
| | | | $\beta = 1.90$ & $V/a^4 = 24^3 \times 48$ | |
| 1p | 0.162876 | +0.0275(04) | 0.0060, **0.0080**, 0.0120, 0.0170, 0.0210, 0.0260 | 450 |
| 1m | 0.163206 | −0.0273(02) | 0.0060, **0.0080**, 0.0120, 0.0170, 0.0210, 0.0260 | 450 |
| 4p | 0.162689 | +0.0398(01) | 0.0060, **0.0080**, 0.0120, 0.0170, 0.0210, 0.0260 | 370 |
| 4m | 0.163476 | −0.0390(01) | 0.0060, **0.0080**, 0.0120, 0.0170, 0.0210, 0.0260 | 370 |

and, for illustrative purposes, Table II shows the pion masses directly obtained from the appropriate ratio of two-point correlators computed for the same ensembles here analyzed.

The lattice spacing values are respectively $a = 0.062(2)$ fm for $\beta = 2.10$, $a = 0.078(3)$ fm for $\beta = 1.95$ and $a = 0.086(4)$ fm for $\beta = 1.90$ [7,8]. Strictly speaking setting the scale in the $N_f = 4$ theory is not plainly well defined. Physical units such as fm or MeV are by definition linked to a physical theory. In practice, as no world containing four light degenerate quarks exists and can produce an experimental observation to compare a lattice result with, the value of $a$ for our setup, as would happen for any other nonphysical one, should result from a convention or assumption. Thus, guided by the assumption that a pion built out of 2 valence quarks of mass $\mu_{\rm val} = \mu_{\rm sea}$

TABLE II. $N_f = 4$ Pseudoscalar masses for the ensembles used in our analysis. The values correspond to the same twisted masses, $a\mu$, of Table I and appear displayed in the same order.

| Ensemble | $am_\pi$ |
|---|---|
| | $\beta = 2.10$ & $V/a^4 = 32^3 \times 64$ |
| 3p | 0.1268(13), **0.1417(11)**, 0.1755(8), 0.2198(7), 0.2516(7), 0.2805(7), 0.3077(7) |
| 3m | 0.1122(22), **0.1332(16)**, 0.1710(13), 0.2161(10), 0.2476(9), 0.2761(8), 0.3028(7) |
| 4p | 0.1462(12), **0.1623(11)**, 0.1958(9), 0.2431(8), 0.2768(8), 0.3078(8) |
| 4m | 0.1304(16), **0.1532(11)**, 0.1910(9), 0.2396(8), 0.2734(7), 0.3042(7) |
| 5p | 0.1606(14), **0.1786(12)**, 0.2051(11), 0.2496(9), 0.2803(9), 0.3088(8) |
| 5m | 0.1424(13), **0.1666(10)**, 0.1967(8), 0.2435(8), 0.2746(7), 0.3032(7) |
| | $\beta = 1.95$ & $V/a^4 = 24^3 \times 48$ |
| 2p | **0.2795(16)**, 0.3107(12), 0.3391(10), 0.3659(9), 0.3909(8) |
| 2m | **0.2630(16)**, 0.2987(12), 0.3287(11), 0.3562(10), 0.3815(9) |
| 3p | 0.2566(18), 0.2678(16),0.2851(14), 0.3016(13), **0.3188(12)**, 0.3318(12), 0.3599(10), 0.3858(9) |
| 3m | 0.1933(12), 0.2196(12), 0.2503(10), 0.2738(9), **0.2956(9)**, 0.3113(9), 0.3434(8), 0.3717(7) |
| 8p | **0.3645(16)**, 0.3723(14), 0.3881(11), 0.4052(10), 0.4232(9), 0.4413(8) |
| 8m | **0.3253(16)**, 0.3364(14), 0.3569(12), 0.3776(11), 0.3985(10), 0.4188(10) |
| | $\beta = 1.90$ & $V/a^4 = 24^3 \times 48$ |
| 1p | 0.3308(13), **0.3362(12)**, 0.3494(12), 0.3698(11),0.3886(10), 0.4132(9) |
| 1m | 0.2912(12), **0.2998(11)**, 0.3183(10), 0.3431(9), 0.3640(8), 0.3902(8) |
| 4p | 0.4032(13), **0.4061(12)**, 0.4138(12), 0.4284(11), 0.4412(11), 0.4598(10) |
| 4m | 0.3492(12), **0.3541(11)**, 0.3653(10), 0.3840(10), 0.4002(9), 0.4218(8) |

living in either the $N_f = 4$ or $N_f = 2 + 1 + 1$ theory acquires the same coupling constant in both cases, the ETMC takes the values of $a$ to be the same for both theories. Corrections to this assumption, which ChPT can in principle account for, should surely exist although they are not expected to be very large. Therefore, as the nonperturbative renormalization of $N_f = 2 + 1 + 1$ lattice QCD in the massless quark limit needs the scale setting for the $N_f = 4$ theory, it is natural to take for the lattice spacing of the latter the one of the $N_f = 2 + 1 + 1$ physical theory (that one is of course also not truly physical, as there is some minor correction from the bottom sea quark, which is however maybe 3 orders of magnitude smaller than the errors of the computation).

Furthermore, in Ref. [11] a novel procedure for the lattice scale setting is proposed and claimed to be particularly in order for relative "calibrations" (ratios of lattice spacings) and for nonphysical cases such as $N_f = 4$ simulations. The very point of the procedure is the scale setting via the intercomparison of a purely gluonic quantity, as the strong coupling in Taylor scheme, which is first assumed and *a posteriori* numerically shown not to depend on the quark masses, at least far away from the flavor thresholds. Applied to the $N_f = 4$ theory [11], the resulting lattice spacings are proven to be compatible with those obtained for ETMC for $N_f = 2 + 1 + 1$ [7,8].

The fixing of the Landau gauge is achieved by the iterative minimization of a functional of the SU(3) links with a combination of stochastic over-relaxation and Fourier acceleration.

## III. RENORMALIZATION CONSTANTS IN THE RI'-MOM SCHEME

In this section we define the notation that we utilize, recall briefly the RI'-MOM scheme [1] and the explicit formulas that will be used in the computation. We refer the reader to Ref. [12] for a complete and pedagogical introduction to the RI'-MOM scheme. The RI'-MOM scheme is very widely used by many lattice collaborations [8,13–17].

### A. Basics of RI'-MOM

We consider a generic bilinear fermion operator $O_\Gamma = \bar{q}_1 \Gamma q_2$ where $\Gamma$ is any Dirac structure, possibly multiplying a covariant derivative operator, and $q_1, q_2$ two fermionic fields. In the case of scalar, pseudoscalar, vector and axial renormalization constants, $\Gamma = 1, \gamma_5, \gamma_\mu, \gamma_5\gamma_\mu$ respectively. To avoid contributions from disconnected diagrams, we focus mainly on the nonsinglet quark operators, unless stated differently. The corresponding renormalized operator is defined as $O_R = Z_O O_\Gamma$, $Z_O$ is found in the RI' variant of the RI-MOM scheme by imposing at a scale $\mu$ large enough (typically $\mu \gg \Lambda_{\rm QCD}$) that the amputated Green function in a fixed gauge (the Landau gauge in our case) equals its tree value, i.e. requiring that

$$Z_O(\mu) Z_q^{-1}(\mu) \Gamma_O(p)|_{p^2=\mu^2} = 1, \tag{5}$$

$Z_q$ is the fermion field renormalization constant, determined through

$$Z_q(\mu^2 = p^2) = -\frac{i}{12p^2} \mathrm{Tr}[S_{bare}^{-1}(p) \not{p}], \tag{6}$$

where $S_{\rm bare}(p)$ is the bare quark propagator. At finite lattice spacing, the four-vector $p$ can be either the continuum momentum, or the lattice momentum $ap_\mu = \sin(ap_\mu)$. Both definitions differ only by $\mathcal{O}(a^2)$ terms. Since RCs obtained using the continuum momentum already exhibit lattice spacing artifacts at tree level, the lattice momentum definition is favored. $\Gamma_O$ is defined in terms of the amputated Green function, or vertex, $\Lambda_O$, by

$$\begin{aligned} \Gamma_O(p) &= \frac{1}{12} \mathrm{Tr}(\Lambda_O(p) \hat{P}_O) \quad \text{with} \\ \Lambda_O(p) &= S_{q1}^{-1}(p) G_O(p) S_{q2}^{-1}(p), \end{aligned} \tag{7}$$

where $\hat{P}_O$ is a suitable projector (see section below) and the Green function is defined in coordinate space by

$$G_O(x, y) = \langle q_1(x) O_\Gamma \bar{q}_2(y) \rangle. \tag{8}$$

On the lattice and in Fourier space, the Green function becomes

$$\begin{aligned} G_O(p) &= \int d^4x d^4y e^{-ip(x-y)} G_O(x, y) \\ &= \frac{1}{N} \sum_i S_{q_1;i}(p|z) \Gamma \gamma_5 S^\dagger_{q_1;i}(p|z) \gamma_5, \end{aligned} \tag{9}$$

where the sum runs over $N$ configurations, $S_i(p|z) = \int d^4y S_i(y, z) e^{-ipy}$ and $\Lambda_O(p)$ in definition equation (7) reads

$$\Lambda_O(p) = S_{q_1}^{-1}(p) G_O(p) \gamma_5 S_{q_1}^{-1\dagger}(p) \gamma_5. \tag{10}$$

It involves only one type of quark propagator since we have taken into account the properties of the twisted-mass formulation relating mass degenerate quarks.

We will study in particular in this work the twist-2 operator $O_{44}$. Twist-2 operators are of particular importance since they provide the leading contribution to the operator product expansion (OPE) analysis of the deep inelastic scattering and this particular one is associated with the $\langle x \rangle_q = \int_0^1 dx x(q(x) + \bar{q}(x))$ of the hadrons [18], where $x$ is the momentum fraction carried by the quark and $q(x)$ the associated longitudinal distribution.

For a general twist-2 operator, $O_\Gamma(z, z') = \bar{q}_1(z) \times \Gamma(z, z') q_2(z')$, we take $\Gamma = \Gamma_\mu \overleftrightarrow{D}_\nu$ with $\overleftrightarrow{D}_\nu = \frac{1}{2}(\nabla_\nu + \nabla^*_\nu)$,

where $\nabla$ and $\nabla^*$ are respectively the gauge covariant forward and backward derivatives, defined by

$$\nabla_\nu(x,y) = a^{-1}(\delta_{y,x+\nu}U_\nu(x) - \delta_{x,y}), \tag{11}$$

$$\nabla^*_\nu(x,y) = a^{-1}(\delta_{x,y} - \delta_{y,x-\nu}U^\dagger_\nu(x-\nu)), \tag{12}$$

where $U$ are the gauge links. Inserting these definitions into the Green function and performing the Wick contractions lead to

$$G_O(x,y) = -\frac{1}{2}\{S_{q_1}(x,z)\gamma_5 S^\dagger_{NL}(y,z)\gamma_5 + S_{NL}(x,z)\gamma_5 S^\dagger_{q_1}(y,z)\gamma_5\}, \tag{13}$$

where we have defined

$$S_{NL}(x,z) = S_{q_1}(x,z+\nu)U^\dagger_\nu(z)\Gamma_\mu - S_{q_1}(x,z-\nu)U_\nu(z-\nu)\Gamma_\mu. \tag{14}$$

This "nonlocal propagator" $S_{NL}$, combining the neighboring propagators, is the solution of a Dirac equation with a modified source

$$\sum_y D(x,y)S_{NL}(y,z) = \delta_{x,z+\nu}U^\dagger_\nu(z)\Gamma_\mu - \delta_{x,z-\nu}U_\nu(z-\nu)\Gamma_\mu, \tag{15}$$

where $D(x,y)$ is the Dirac operator. Using these nonlocal propagators, from which we can construct all $\Gamma$ structures, we decrease the number of propagators to be computed, from nine to five (1 with a "local" source and 4—one in each direction—with a nonlocal one). The advantage of our method is thus the reduced computational cost, since with only 5 inversions per configuration, we are able to extract all local and twist-2 renormalization constants for all momenta.

Finally, the Green function in momentum space becomes

$$G_O(p) = -\frac{1}{2}\cdot\frac{1}{N}\sum_i\{S^{q_1}_i(p|z)\gamma_5 S^{q_1\dagger}_{i,NL}(p|z)\gamma_5 + S^{q_1}_{i,NL}(p|z)\gamma_5 S^{q_1\dagger}_i(p|z)\gamma_5\}. \tag{16}$$

### B. Projectors

For scalar and pseudoscalar operators, the projector $\hat{P}_O$ in (7) is simply $\gamma_0$ and $\gamma_5\gamma_0$ respectively. For vector and axial vertex functions however, "naïve projectors" $\gamma_\mu$ and $\gamma_5\gamma_\mu$ do not project vertices onto different Lorentz structures. Indeed, the vertex function decomposes over the Dirac structures as

$$\Gamma^V_\mu = \Sigma^V_1\gamma_\mu + \Sigma^V_2\frac{p_\mu}{p^2}\not{p}, \tag{17}$$

$$\Gamma^A_\mu = \Sigma^A_1\gamma_5\gamma_\mu + \Sigma^A_2\gamma_5\frac{p_\mu}{p^2}\not{p}, \tag{18}$$

with $\Sigma^V_{1,2}$ and $\Sigma^A_{1,2}$ being scalars multiplied by $3\times 3$ identity matrices which we omit to simplify the notation. The correct projectors are actually given by

$$P^V_\mu = \gamma_\mu - \frac{p_\mu}{p^2}\not{p},$$
$$P^A_\mu = \gamma_5\gamma_\mu - \gamma_5\frac{p_\mu}{p^2}\not{p}, \tag{19}$$

and the corresponding form factors are then

$$\Sigma^{A/V}_1 = \frac{1}{12}\frac{p^2}{p^2-p^2_\mu}\mathrm{Tr}[P^{A/V}_\mu\Gamma^{A/V}_\mu]. \tag{20}$$

We have checked that the effect of using or not using these correct projectors has a rather small influence on $Z_V$ and $Z_A$. However, since statistical errors will turn out to be also small, we will use in what follows the correct projectors of Eq. (19).

In a similar way, twist-2 operators should be projected such that Lorentz structures are decoupled. Following the convention used in Ref. [19], we define a general symmetric and traceless twist-2 operator as

$$O_{\mu\nu} = \gamma_\mu D_\nu + \gamma_\nu D_\mu - \frac{1}{2}\delta_{\mu\nu}\gamma_\rho D^\rho. \tag{21}$$

The corresponding Green function can be decomposed as

$$G_O = -\frac{1}{2}\Sigma_1(p)\left(\gamma_\mu p_\nu + \gamma_\nu p_\mu - \frac{1}{2}\delta_{\mu\nu}\not{p}\right) - \Sigma_2(p)\not{p}\left(p_\mu p_\nu - \frac{1}{4}p^2\delta_{\mu\nu}\right). \tag{22}$$

To project out the first form factor $\Sigma_1(p)$ we use (correcting minor typos in Ref. [19])

$$P_O = -p^2\frac{\left(\frac{p_\mu p_\nu\not{p}}{p^2} - \frac{(\gamma_\mu p_\nu+\gamma_\nu p_\mu)}{2}\right)}{(4p^2_\mu p^2_\nu - p^2(p^2_\mu+p^2_\nu) - 2p_\mu p_\nu p^2\delta_{\mu\nu})}. \tag{23}$$

In particular, in the case of $O_{44}$ operator, we obtain

$$P_O = p^2\frac{\left(\frac{p^2_4\not{p}}{p^2} - \gamma_4 p_4\right)}{4p^2_4(\vec{p}^2)}. \tag{24}$$

## IV. ANALYSIS PROCEDURE

For each value of the sea quark mass, two sets of gauge fields are produced, with opposite $m_{PCAC}$ values, corresponding to opposite values of the angle $\theta$, the latter being defined as the complementary to the twisted angle, see

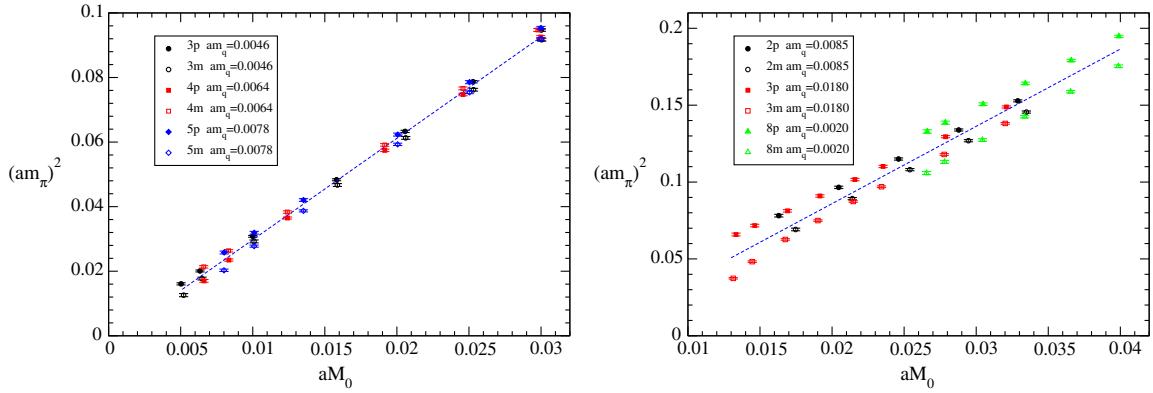


FIG. 1 (color online). Pion mass for each $\beta = 2.10$ (lhs) and $\beta = 1.95$ (rhs) ensemble, before $\theta$ average. The $x$-axis is the renormalized quark mass $M_0 = \sqrt{(Z_A m_{\mathrm{PCAC}})^2 + m_q^2}$ and the $y$-axis is the pion mass squared, both in lattice units. The difference between m/p ensembles illustrates the consequence of nonmaximal twist and $\mathcal{O}(a)$ effects. The result of the straight line fit using pion mass values computed after $\theta$ average is shown in dashed blue curve.

Ref. [7]. The first step consists in removing the Goldstone pole from vertex functions, for each ensemble, and in performing the valence quark mass extrapolation. The $\theta$ average is then done, before correcting for $H(4)$ artifacts. The different steps of the analysis are detailed below using a given set of ensembles, namely $3p/3m$ ensembles on a $32^3 \times 64$ lattice. The results presented in the next two sections concern charged currents and densities: $O = \bar{u}\Gamma d$ or $O = \bar{d}\Gamma u$. All plots in this section represent average of jackknife bins and statistical errors appear also estimated by the jackknife method. A sensible full-correlated-matrix analysis would require much higher statistics than the one from the available data. This is why we proceed otherwise and apply the jackknife approach for the error analysis also followed in a series of papers [2,3,5,16,20,21], devoted in the last few years to the study of the nonperturbative running of renormalization constants, and that revealed itself as very useful for dealing with the fits of correlated parameters. Although the meaning for the $\chi^2$/d.o.f. estimates are purely indicative and only useful for comparative purposes, the estimated errors from the jackknife bins for the fitted parameters appear to be meaningful.

### A. Pion mass and Goldstone pole subtraction

For each ensemble, the first step of the RCs analysis consists in subtracting the Goldstone pole contribution on vertex functions. This requires us to compute the pion mass for each configurations' set. Pion masses are determined before performing the $\theta$ average. The results are illustrated in Fig. 1, showing the pion mass as a function of the renormalized quark mass $M_0 = \sqrt{(Z_A m_{\mathrm{PCAC}})^2 + m_q^2}$ where an estimate of $Z_A = 0.78(0.73)$ has been taken for $\beta = 2.10$ from Ref. [7] (and $\beta = 1.95$ from Ref. [22]).

After the jackknife bins of vertex functions (or $Z_q$, for the quark wave function renormalization constant) have been computed, an average over $H(3)$ invariants is performed. Then the Goldstone pole subtraction is done, bin by bin and before the $\theta$ average. The pole is taken as the charged pion mass squared at nonmaximal twist

$$\Gamma(p^2, \mu_{\mathrm{sea}}) = A(p^2) + B(p^2) m_\pi^2 + \frac{C(p^2)}{m_\pi^2}, \qquad (25)$$

where $C(p^2)$ is the nonperturbative Goldstone pole contribution [23]. The value of the subtracted vertex functions $\bar{u}\Gamma d$ and $\bar{d}\Gamma u$ extrapolated to zero mass are very similar. This justifies the average over nonsinglet operators that will be performed later in the analysis. As we only consider charged vertices, there is to our knowledge no coupling to any neutral Goldstone pole. The extrapolation to the chiral limit of RCs, instead of being performed in term of the quark masses, is done in function of the pion mass. There is strong corroborative evidence, based on the vacuum saturation approximation in support of the fact that the charged pion mass is much less affected by $\mathcal{O}(a^2)$ effects than the neutral pion mass [24]. The important statement is that the dominant contamination of the charged vertices in question comes from the charged pion. This is also shown explicitly in [12]. Of course, there are neutral pions in the sea, but whatever contribution they give must be subdominant.

Only the pseudoscalar vertex is expected to exhibit a Goldstone pole. We have however also inspected other vertices to check possible contamination or lattice artifacts. On Fig. 2 for the $3p$ ensemble, the scalar vertex functions for the $u$ quark are plotted (filled symbols) versus the pion mass squared and compared with the subtracted values (empty circles). The extrapolated value is also indicated (star symbol). The difference between subtracted and nonsubtracted values lies at the fourth digit for all valence quark masses for $a^2\vec{p}^2 \geq \sim 0.5$, and it is not visible on the plot. For lower $a^2\vec{p}^2$ values however, the subtraction effect

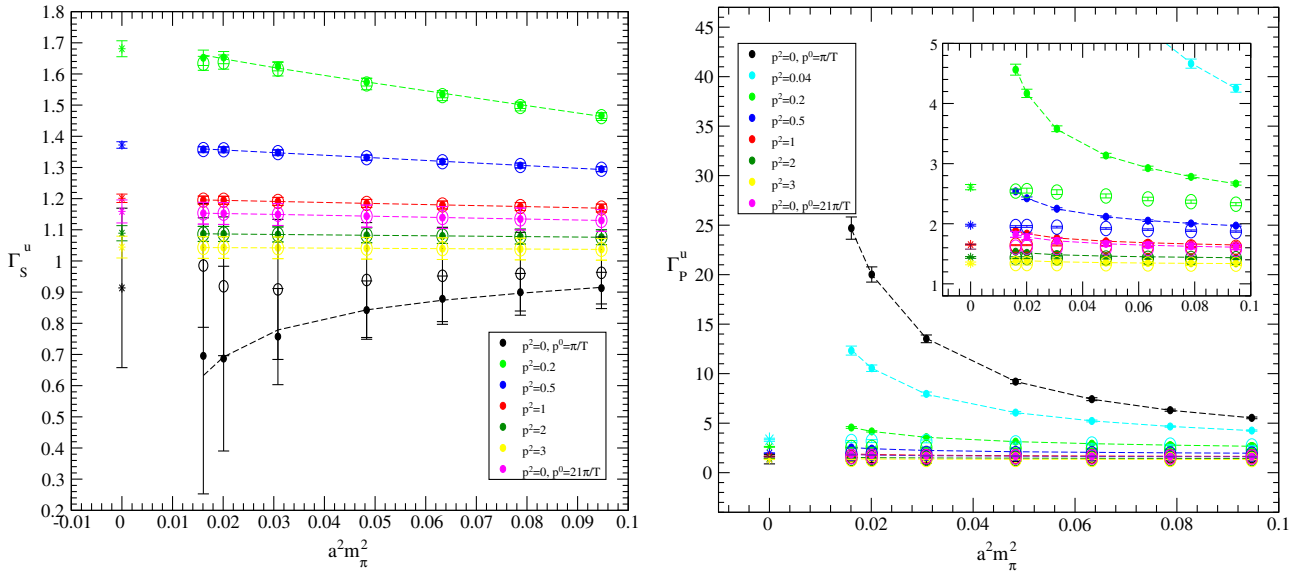


FIG. 2 (color online). $\bar{d}\Gamma u$ scalar (lhs) and pseudoscalar (rhs) vertex functions versus pion mass squared (in lattice units) for ensemble $3p$ ($\beta = 2.10$) for several values of $a^2\vec{p}^2$ ($ap^0 = \frac{\pi}{T}$ for all curves except the magenta one, for which $ap^0 = \frac{21\pi}{T}$).

is visible. Since no Goldstone pole contamination is expected for $Z_S$ [12], those effects are likely to be lattice artifacts. A similar conclusion holds for the quark renormalization constant and for the vector current. The axial vector current also has a coupling to the pion and this could be potentially a source of a problem but since this coupling is proportional to the momentum transfer of the process, which actually vanishes for our kinematical setup, it poses no problem either [25,26].

We stress that, since the low values of $a^2\vec{p}^2$ will be excluded from the fit range considered when compensating for $H(4)$ artifacts (see next section), these lattice effects will not influence the final results.

Contrary to $\Gamma_S$, the pseudoscalar vertex function shows, as expected, a strong pion mass dependence. Vertex functions for ensembles $3p$ are displayed in the rhs of Fig. 2, with the same legend conventions as for the plots of the scalar vertex. The Goldstone pole appears clearly and is thus subtracted according to Eq. (25).

The $p^2$ dependence of the chiral extrapolation coefficients are displayed in Fig. 3. The $1/m_\pi^2$ coefficient of the chiral extrapolation is, as expected, varying as $1/p^2$ for

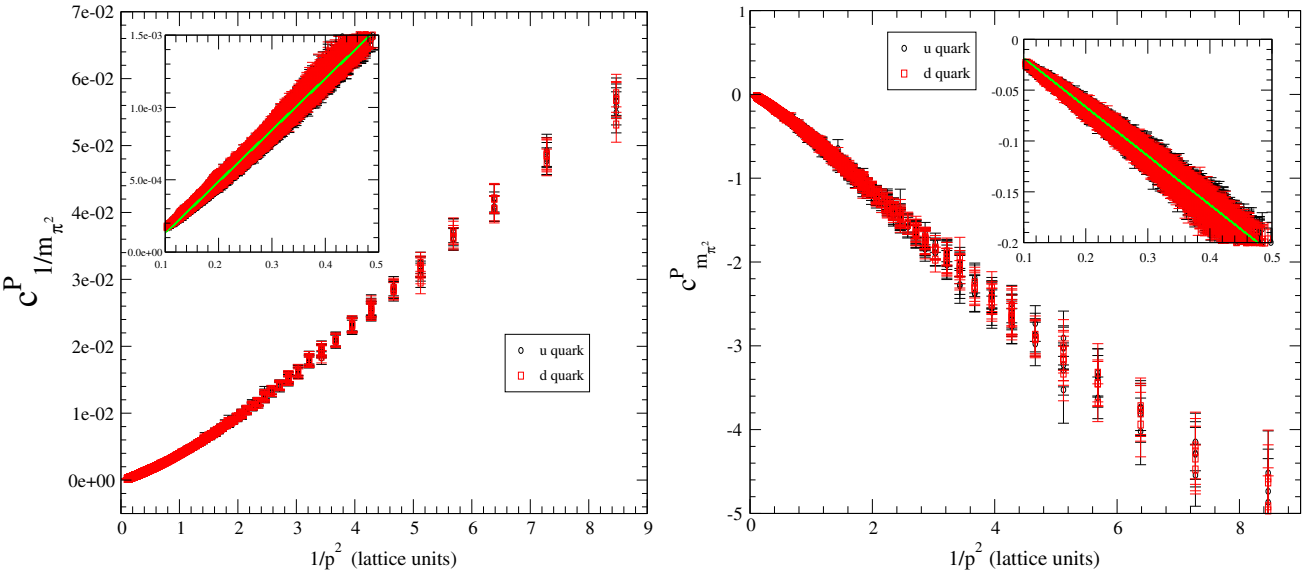


FIG. 3 (color online). Coefficient of the $1/m_\pi^2$ term (lhs) and of the $m_\pi^2$ term (rhs) in the chiral fit [in (25), $C(p^2)$ and $B(p^2)$ resp.] as a function of $1/p^2$ in lattice units, for ensemble $3p$ ($\beta = 2.10$). The green line serves as eye guidance mainly and represents a linear fit at large $p^2$.

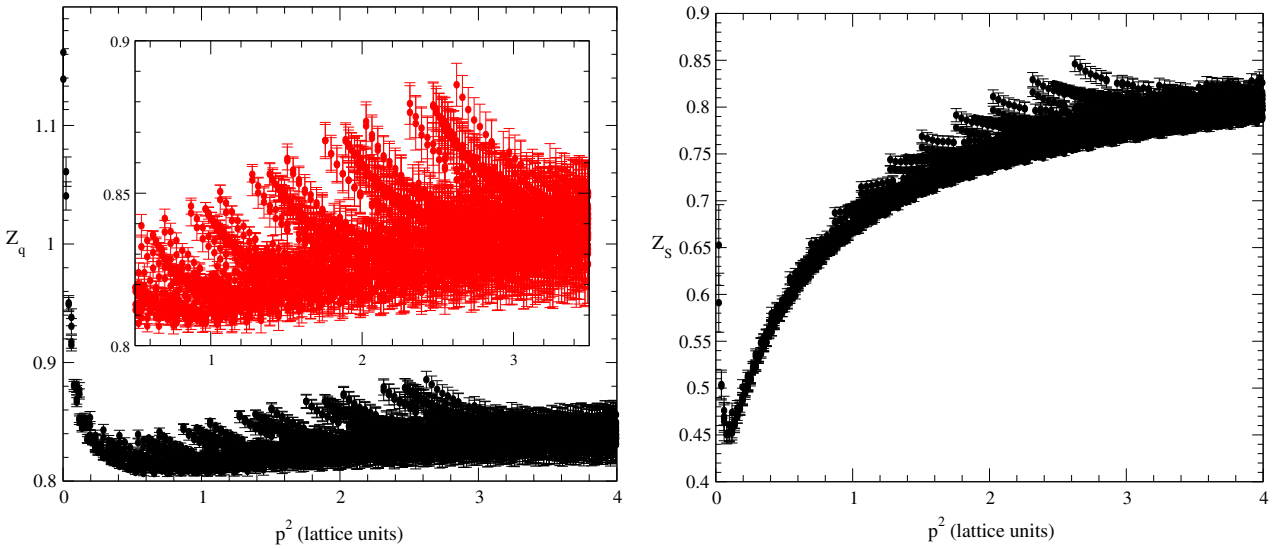


FIG. 4 (color online). Quark renormalization constant (lhs) and scalar renormalization constant (rhs) as a function of $p^2$ in lattice units. Both exhibit the typical fishbone structure induced by the breaking of the $O(4)$ rotational symmetry of the Euclidian space-time by the lattice discretization, into the hypercubic group $H(4)$.

pseudoscalar vertex, at large $p^2$. Over the large range of $a^2p^2$ values considered (typically for $a^2p^2 > 0.1$), this coefficient varies as $c_1/p^2 + (c_2/p^2)^2$. This is consistent with the expectation that the Goldstone pole can only appear in power suppressed nonperturbative contributions. For other vertices, it is globally compatible with zero.

### B. $m_{PCAC}$ average and hypercubic corrections

The $m_{PCAC}$ average is performed on the vertex function jackknife bins. Since they differ only by (small) lattice artifacts, nonsinglet operators ($\bar{u}Od$ and $\bar{d}Ou$) are also averaged at this stage, with an average weighted by jackknife errors. The scalar (rhs) and quark wave function (lhs) renormalization constants are represented for the representative pair ensembles $3m/3p$ (see Table I) in Fig. 4 as a function of $p^2 = p_\mu p^\mu$, in lattice units. $Z_q$ exhibits the usual strong half "fishbone" structure, typical of hypercubic artifacts, while other renormalization constants are also affected, although to a lesser extent.

The three vector components $\gamma_\mu$ (and similarly for the three axial ones $\gamma_\mu\gamma_5$) being very similar (not shown on these figures) and degenerate in the continuum limit, they are also averaged before hypercubic artifacts are removed.

The next step consists in correcting one of the two types of $\mathcal{O}(a^2)$ artifacts, namely the hypercubic artifacts which respect the $H(4)$ symmetry group but not the $O(4)$ one [the second type, i.e. $\mathcal{O}(a^2p^2)$ artifacts, respecting the continuum $O(4)$ rotation symmetry, will be treated nonperturbatively by introducing corrections in the running of the RCs, see Sec. V]. A very powerful method has been developed [2,4], which does not rely on the selection of a small subset of momenta, thus keeping the maximum amount of information. A byproduct of this procedure is the fact that, unlike other methods, it allows us to test the running of the renormalization constants. This method has already been extensively and fruitfully exploited in studying the QCD running coupling [20,21,27–30] or the gauge fields propagators [2,31,32], while its applications to renormalization have been presented in detail in [3,16,33]. It will only be recalled here briefly for the sake of consistency. We define the following $H(4)$ invariants:

$$p^{[2]} = \sum_{\mu=1}^{4} p_\mu^2, \qquad p^{[4]} = \sum_{\mu=1}^{4} p_\mu^4,$$
$$p^{[6]} = \sum_{\mu=1}^{4} p_\mu^6, \qquad p^{[8]} = \sum_{\mu=1}^{4} p_\mu^8, \tag{26}$$

and denote the quantity $Z(ap_\mu)$ (representing any renormalization constant) averaged over the cubic orbits as $Z_{\text{latt}}(a^2p^2, a^4p^{[4]}, a^6p^{[6]}, ap_4, a^2\Lambda^2_{\text{QCD}})$. We then assume (and will check) that $Z_{\text{latt}}$ can be Taylor expanded around $p^{[4]} = 0$ up to values of $\epsilon = a^2p^{[4]}/p^2$ significantly larger than 1 as

$$Z_{\text{latt}}(a^2p^2, a^4p^{[4]}, a^6p^{[6]}, ap_4, a^2\Lambda^2_{\text{QCD}}) = Z_{\text{hypcorrected}}(a^2p^2, ap_4, a^2\Lambda^2_{\text{QCD}}) + R(a^2p^2, a^2\Lambda^2_{\text{QCD}})\frac{a^2p^{[4]}}{p^2} + \ldots, \tag{27}$$

with

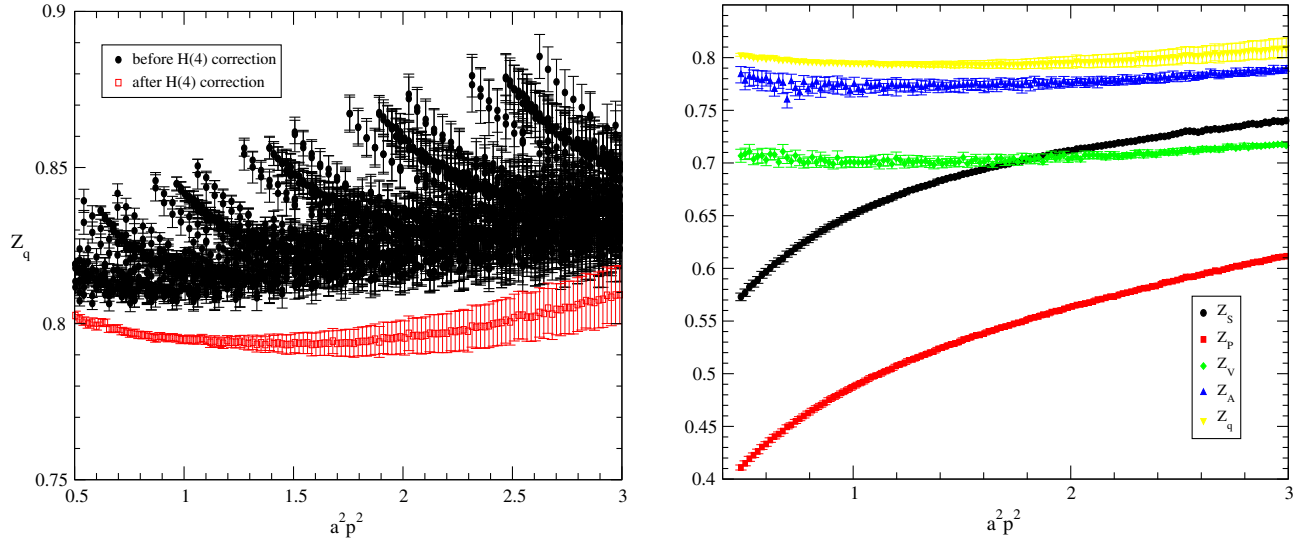


FIG. 5 (color online). lhs: Effect of hypercubic corrections on quark renormalization constant, as a function of $a^2p^2$, for ensemble $3mp$ ($\beta = 2.10$, $\mu_{\rm sea} = 0.0046$, $32^3 \times 64$ lattice). rhs: Renormalization constants as a function of $a^2p^2$, after removing $H(4)$ artifacts, still for ensemble $3mp$ ($\beta = 2.10$, $\mu_{\rm sea} = 0.0046$, $32^3 \times 64$ lattice).

$$R(a^2p^2, a^2\Lambda_{\rm QCD}) = \left.\frac{dZ_{\rm latt}(a^2p^2, a^4p^{[4]}, a^6p^{[6]}, ap_4, a^2\Lambda^2_{\rm QCD})}{d\epsilon}\right|_{\epsilon=0}, \quad (28)$$

$R(a^2p^2, a^2\Lambda_{\rm QCD})$ being reasonably well approximated by $R(a^2p^2, a^2\Lambda^2_{\rm QCD}) = c_{a2p4} + c_{a4p4}a^2p^2$. We use the one window fit technique, described in detail in [16]. The fitting range in $a^2p^2$ is chosen to be [0.5–3]. For values of $a^2p^2$ larger than ≈3, some orbits start indeed to be missing because the Fourier transform equation (9) has been limited to $[-\frac{\pi}{2}, +\frac{\pi}{2}]$. The effect of the hypercubic correction is clearly seen for $Z_q$, on the lhs of Fig. 5. The same procedure is applied to all renormalization constants, leading to the results of Fig. 5 (rhs), which summarizes the results of all local RCs as a function of $a^2p^2$. The hypercubic correction can be applied either at the vertex level, or, as we did, directly on the renormalization constants. We checked that there is no significant difference between these two choices.

The analysis for twist-2 operators is similar (except for the valence quark mass extrapolation) and applied here to $O_{44}$. Figure 6 displays the renormalization constant for $Z_{44}$ before and after the hypercubic corrections. The fishbone structure is about twice more pronounced than for $Z_q$ for instance.

Finally, we note that there are ultraviolet artifacts which are functions of $a^2p^2$ and are thus insensitive to hypercubic biases and not corrected by the above-mentioned method. They will be corrected simply by assuming $a^2p^2$ terms in the final running fit.

As a summary, our analysis procedure to extract renormalization constants consists in the following steps:

(i) the $H(3)$ average of the vertex functions over $\vec{p}^2$ orbits,
(ii) the $1/m_\pi^2$ term subtraction and valence chiral extrapolation, also done at the level of the vertex function, for each four-momentum,
(iii) the $\theta$ average, performed on $Z_q$ or at the vertex level for other renormalization constants,
(iv) the average over nonsinglet $\bar{u}Od$ and $\bar{d}Ou$ operators, weighted by jackknife errors,
(v) the average over equivalent $\mu$ (= 1, 2, 3) directions for vector and axial operators,

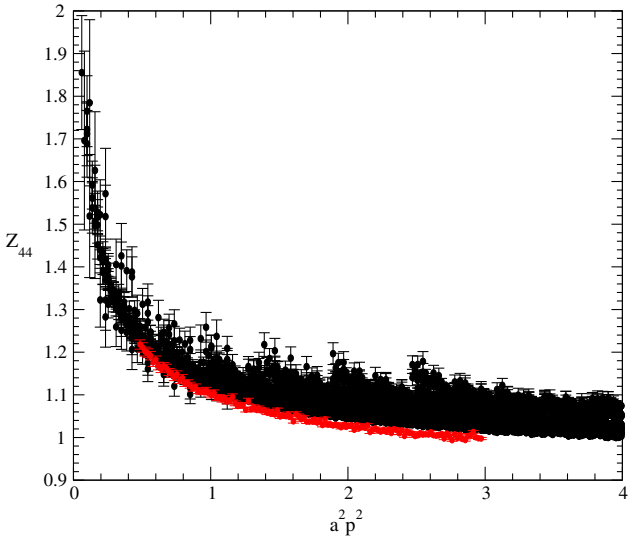


FIG. 6 (color online). Effect of hypercubic corrections on $Z_{44}$, as a function of $a^2p^2$, for ensemble $3mp$ ($\beta = 2.10$, $\mu_{sea} = 0.0046$, $32^3 \times 64$ lattice).

(vi) the correction of hypercubic artifacts using an efficient and well-defined procedure.

The running of the RCs will be described in details in the next section.

## V. RUNNING AND $\mathcal{O}(a^2p^2)$ ARTIFACTS

The possibility to check the running of renormalization constants is an important feature of our analysis. This allows us to study remaining lattice artifacts and nonperturbative contributions and to finally extract reliable values of the RCs.

### A. Renormalization constants for quark and local operators

We consider the following expression for the running of the quark wave function RC:

$$Z_q^{\mathrm{hyp-corr}}(a^2p^2) = Z_q^{\mathrm{pert}RI'}(\mu^2)c_{0Z_q}^{RI'}\left(\frac{p^2}{\mu^2},\alpha(\mu)\right) \times\left(1+\frac{\langle A^2\rangle_{\mu^2}}{32p^2}\frac{c_{2Z_q}^{\bar{M}S}(\frac{p^2}{\mu^2},\alpha(\mu))}{c_{0Z_q}^{RI'}(\frac{p^2}{\mu^2},\alpha(\mu))}\frac{c_{2Z_q}^{RI'}(\frac{p^2}{\mu^2},\alpha(\mu))}{c_{2Z_q}^{\bar{M}S}(\frac{p^2}{\mu^2},\alpha(\mu))}\right) + c_{a2p2}a^2p^2 + c_{a4p4}(a^2p^2)^2, \quad (29)$$

which was derived in Ref. [16] using an OPE analysis. The coefficients $c_{0Z_q}^{RI'}$ and $c_{2Z_q}^{\bar{M}S}$ are known from perturbation theory and the running formula contains lattice artifact terms $\propto a^2p^2$ and $\propto (a^2p^2)^2$, not yet removed. These additional terms are discussed below. We are left with four parameters to determine, namely the value of the RC $Z_q^{\mathrm{pert}RI'}(\mu^2)$ at a given renormalization scale $\mu$, the dimension-2 Landau gauge gluon condensate $\langle A^2\rangle_{\mu^2}$ and the coefficients $c_{a2p2}$ and $c_{a4p4}$. The expression (29) includes, apart from the corrections accounting for the not-yet-removed artifacts, the nonperturbative power correction, $1/p^2$, generated by the nonvanishing gluon condensate [5,6]. The same nonperturbative contributions have been previously proven to be mandatory when describing the running of gluon, ghost and quark propagators renormalization constants [5,30,31,33]. We find here, as will be illustrated below, that Eq. (29), nothing less but nothing more, perfectly describes the quark wave function. For the other renormalization constants we also deal with, the same nonvanishing gluon condensate must contribute, *via* their corresponding OPE expansion, to generate the same nonperturbative power corrections, unless the Wilson coefficient is proven to be zero. However, even for the latter case, other possible nonperturbative corrections as the pion pole for $Z_P$, hadron contributions or lattice artifacts may also contribute and be hardly disentangled from the OPE ones, with the present level of precision. Then, as will be seen in the following, for renormalization constants other than the quark wave function, we will apply a power correction in lattice units, $1/p^2_{\mathrm{latt}} = 1/a^2p^2$, and will not distinguish the different possible sources for its origin. The coefficient of this correction is $a$ dependent and is such that cancels the naive divergence. Unfortunately, due to the fact that we only have three different values of the lattice spacing in the available ensembles we cannot perform an accurate fit in order to determine the functional behavior of this coefficient.

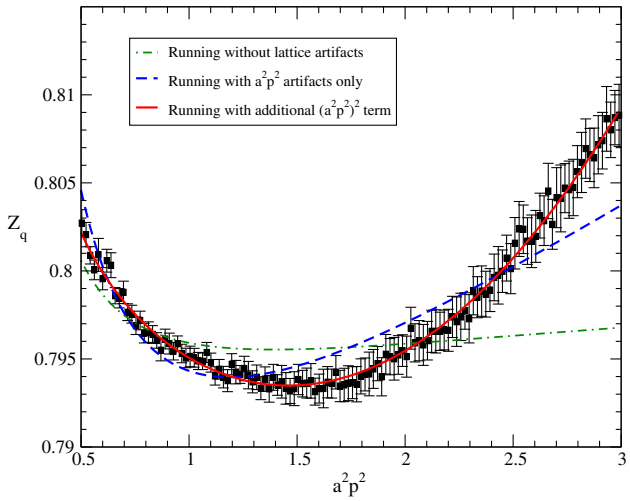


FIG. 7 (color online). Running of $Z_q$ for ensemble $3mp$ ($\beta = 2.10$, $\mu = 0.0046$, volume $32^3 \times 64$) using different fitting formulas.

We illustrate below the results for $Z_q$ with the ensemble $3mp$, which is representative of the results we obtained with all other ensembles. We take $\Lambda_{\mathrm{QCD}} = 316$ MeV from Ref. [28] and $a_{\beta=2.10} = 0.062$ fm from Ref. [7]. The results for local renormalization constants are not sensitive to these values and changing $a$ and $\Lambda_{\mathrm{QCD}}$ over a wide range induces only a change in the local RC's values on the last digit. This however is not the case for twist-2 operators (see Sec. V B).

Figure 7 displays the running of $Z_q$ for the ensemble $3mp$, fitted by different formulas, depending on whether or not lattice artifacts are included in the running. It can be shown that the standard OPE expression without any artifact correction (dot-dashed green curve) fails completely to describe the data. Adding only an $a^2p^2$ term decreases the $\chi^2$/d.o.f. down to 2.85 but the running is still not correctly reproduced. The $\chi^2$/d.o.f. can be, even more, diminished if the fitting window is restricted down to lower momenta. However, as the $H(4)$-extrapolation has been proved to deal properly with hypercubic artifacts for $Z_q$ up to higher momenta, $a^2p^2 \sim (\pi/2)^2 \sim 2.5$ [16,33], we prefer to add only one more parameter to be fitted, including both $a^2p^2$ and $(a^2p^2)^2$ terms accounting for $O(4)$-invariant artifacts, to obtain a good fit over the whole range of momenta. The running is then very well described

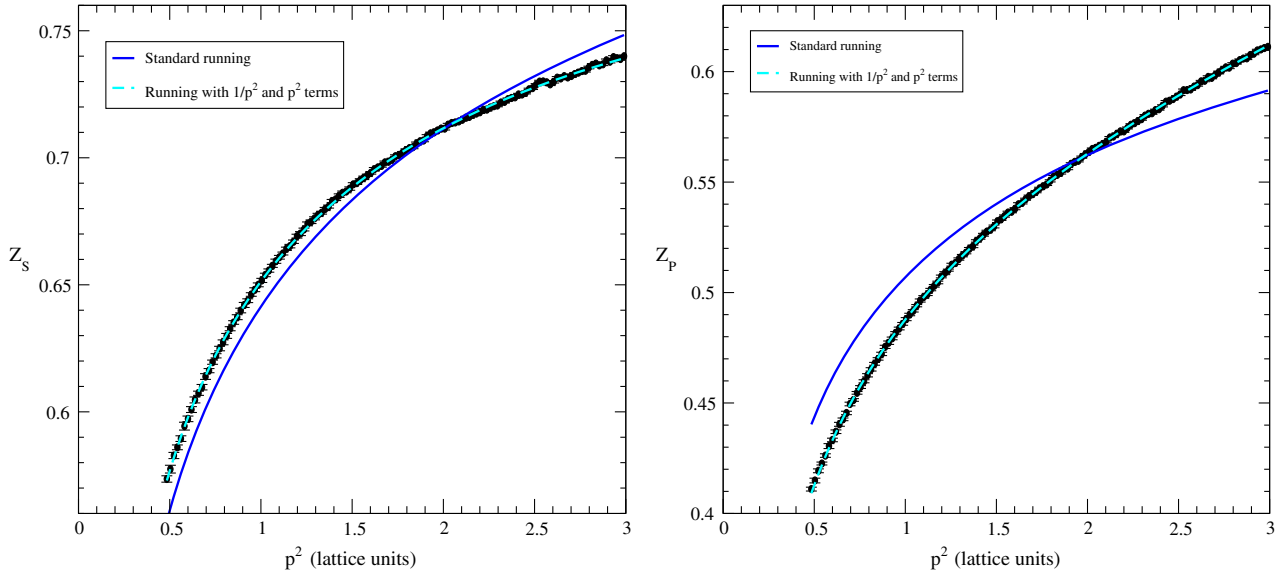


FIG. 8 (color online). lhs: Running of $Z_S$ for ensemble $3mp$ ($\beta = 2.10$, $\mu = 0.0046$, volume $32^3 \times 64$). The standard running formula is represented in solid blue line, the dashed cyan curve includes an $1/p^2$ and an $p^2$ term (in lattice units). This latter fit leads to $Z_S(10\ \mathrm{GeV}) = 0.869(4)$. rhs: Running of $Z_P$ with the standard running expression from (30) (solid blue curve), and adding a $1/p^2$ and a $p^2$ terms (in lattice units, dashed cyan curve). The modified running gives $Z_P(10\ \mathrm{GeV}) = 0.623(2)$.

($\chi^2/\mathrm{d.o.f.} = 0.26$) and we get at 10 GeV $Z_q(\mu = 10\ \mathrm{GeV}) = 0.815(10)$. Errors quoted are at the moment only statistical. Precise estimations of the systematic errors will be performed in Sec. VIII.

The same study is performed for scalar and pseudoscalar RCs. $Z_S$ and $Z_P$ have the same running formula, namely

$$Z_{P/S}(\mu) = Z_{P/S}(\mu_0)\frac{c^{RI'MOM}(\mu)}{c^{RI'MOM}(\mu_0)} + c_{a2p2}a^2p^2 + \frac{c_{p2m1}}{a^2p^2}, \tag{30}$$

where we have added $1/(a^2p^2)$ and $a^2p^2$ lattice artifact terms. We have [34]

$$\begin{aligned} c^{RI'MOM}(\mu) = x^{\bar{\gamma}_0}\Big\{ & 1 + (\bar{\gamma}_1 - \bar{\beta}_1\bar{\gamma}_0)x + \frac{1}{2}[(\bar{\gamma}_1 - \bar{\beta}_1\bar{\gamma}_0)^2 + \bar{\gamma}_2 + \bar{\beta}_1^2\bar{\gamma}_0 - \bar{\beta}_1\bar{\gamma}_1 - \bar{\beta}_2\bar{\gamma}_0]x^2 \\ & + \Big[\frac{1}{6}(\bar{\gamma}_1 - \bar{\beta}_1\bar{\gamma}_0)^3 + \frac{1}{2}(\bar{\gamma}_1 - \bar{\beta}_1\bar{\gamma}_0)(\bar{\gamma}_2 + \bar{\beta}_1^2\bar{\gamma}_0 - \bar{\beta}_1\bar{\gamma}_1 - \bar{\beta}_2\bar{\gamma}_0) \\ & + \frac{1}{3}(\bar{\gamma}_3 - \bar{\beta}_1^3\bar{\gamma}_0 + 2\bar{\beta}_1\bar{\beta}_2\bar{\gamma}_0 - \bar{\beta}_3\bar{\gamma}_0 + \bar{\beta}_1^2\bar{\gamma}_1 - \bar{\beta}_2\bar{\gamma}_1 - \bar{\beta}_1\bar{\gamma}_2)\Big]x^3 + \mathcal{O}(x^4)\Big\}, \end{aligned} \tag{31}$$

where $x = \alpha$, $\bar{\gamma}_i = \gamma_i/\beta_0$ and $\bar{\beta}_i = \beta_i/\beta_0$. $\beta_i$ are the coefficients of the QCD beta function and they are given at four-loop in [34]. Their expressions for scalar, pseudoscalar operators and quark propagator can be written [13,35]

$$\beta_0 = 11 - \frac{2}{3}N_f, \qquad \beta_1 = 102 - \frac{38}{3}N_f,$$
$$\beta_2 = \frac{2857}{2} - \frac{5033}{18}N_f + \frac{325}{54}N_f^2,$$

and the anomalous dimensions $\gamma_i$ are given below

$$\gamma_0^{S/P} = -3C_F, \qquad \gamma_1^{S/P} = \frac{1}{2}\left(-\frac{404}{3} + \frac{40}{9}N_f\right),$$
$$\gamma_2^{S/P} = \frac{1}{2}\left(-2498 + \left(\frac{4432}{27} + \frac{320}{3}\zeta(3)\right)N_f + \frac{280}{81}N_f^2\right).$$

As for the quark renormalization constant, the standard running formula, i.e. Eq. (30) without $1/p^2_{\mathrm{latt}}$ and $p^2_{\mathrm{latt}}$ terms, fails to describe the running of both $Z_S$ and $Z_P$, as illustrated in Fig. 8 (solid blue curves), though to a lesser extent than for $Z_q$. Additional terms are needed to take into account $\mathcal{O}(a^2p^2)$ artifacts. The evolution of scalar

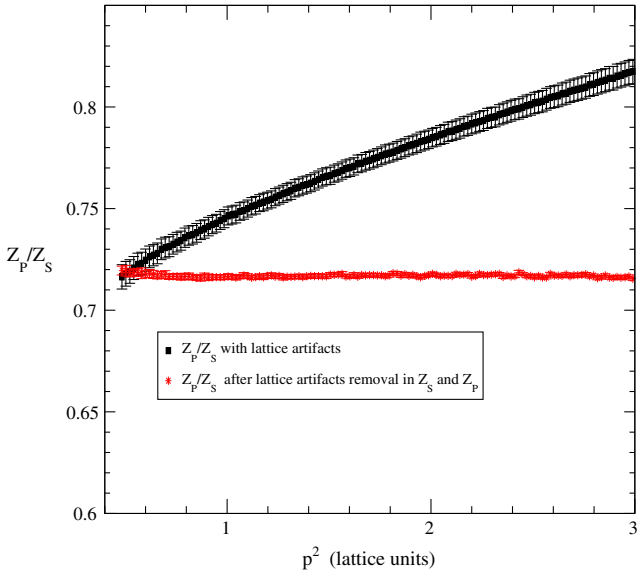


FIG. 9 (color online). $Z_P/Z_S$ for ensemble $3mp$ ($\beta = 2.10$, $\mu = 0.0046$, volume $32^3 \times 64$). Lattice artifacts have been removed separately from $Z_S$ and $Z_P$. The ratio of these two RCs is compatible with a constant over the whole $p^2$ interval considered and $Z_P/Z_S = 0.717(3)$.

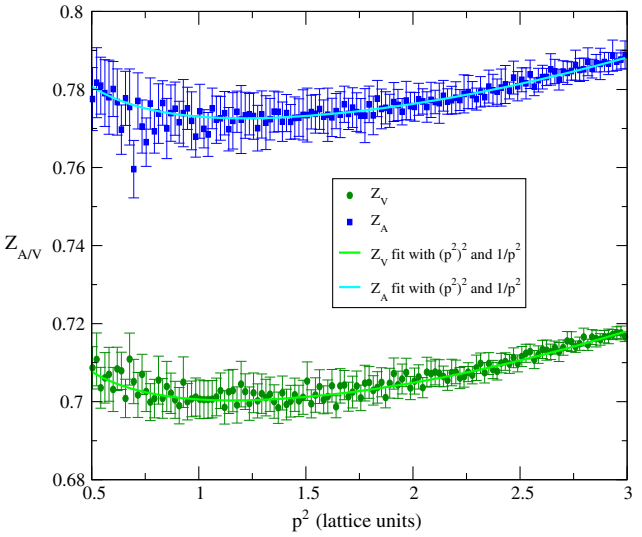


FIG. 10 (color online). Fits of the residual $p^2_{\text{latt}}$ dependence of $Z_V$ and $Z_A$ for ensemble $3mp$ ($\beta = 2.10$, $\mu = 0.0046$, volume $32^3 \times 64$).

and pseudoscalar RCs can be perfectly reproduced with $1/p^2_{\text{latt}}$ and $p^2_{\text{latt}}$ terms added to the standard running by fitting coefficients $c_{a2p2}$ and $c_{p2m1}$, leading to the dashed cyan curves in Fig. 8 ($\chi^2/\text{d.o.f.} = 1.14$ and $\chi^2/\text{d.o.f.} = 0.74$ for respectively $Z_S$ and $Z_P$). The scalar and pseudoscalar RCs values obtained at 10 GeV for this ensemble are $Z_S(\mu = 10\ \text{GeV}) = 0.869(4)$ and $Z_P(\mu = 10\ \text{GeV}) = 0.623(2)$.

Scalar and pseudoscalar RCs having the same anomalous dimension, are expected to have similar running and their ratio should be constant. If $Z_P/Z_S$ is computed without properly taking into account lattice artifacts, the ratio varies by more than 20% on the momentum range considered (see Fig. 9, black circles). However, once $\mathcal{O}(a^2p^2)$ artifacts have been separately removed from $Z_S$ and $Z_P$, the ratio becomes compatible with a constant with very good accuracy, over the whole range of $p^2_{\text{latt}}$ values (see Fig. 9, red stars). This is an additional indication that lattice artifacts have been efficiently removed but also that the Goldstone pole has been correctly addressed.

Axial and vector renormalization constants do not run but it turns out that they exhibit a small $p^2_{\text{latt}}$ dependence, which is not surprising since all other local RCs also show this feature. Their variation does not reach more than 4% in total on the momentum range considered, but to extract reliable values of $Z_V$ and $Z_A$, we remove these artifacts by fitting this dependence, which turns out to be well described by a combination of $1/p^2_{\text{latt}}$ and $(p^2_{\text{latt}})^2$ terms. The results of the fit are shown in Fig. 10, and lead to values $Z_V = 0.688(5)$ and $Z_A = 0.761(4)$.

Table III summarizes the values obtained for local RCs, for all $N_f = 4$ ensembles considered.

In order to estimate the uncertainties on the RCs, coming from the lattice spacing determination, we vary $a$ by 5%, which corresponds to the difference between the lattice spacing determined using either pion data or nucleon data [8,17]. We check the influence of this variation on $Z_q$, $Z_S$, $Z_P$ and $Z_P/Z_S$ for a given ensemble, namely $2mp$, $\beta = 1.95$. Results are summarized in Table IV. Scalar and pseudoscalar $Z$ factors are the most sensitive to the lattice spacing, whereas $Z_q$ varies less than one percent and as expected the ratio $Z_P/Z_S$ is remarkably constant.

### B. Twist-2 operators

The running expression used for $Z_{44}$ is the same than for $Z_S$ [cf. Ref. [34], Eq. (70)]

$$Z_{44}(\mu) = Z_{44}(\mu_0)\frac{c^{RI'MOM}(\mu)}{c^{RI'MOM}(\mu_0)} + c_{a2p2}a^2p^2 + \frac{c_{p2m1}}{a^2p^2}, \tag{32}$$

and with [34]

$$\begin{aligned} c^{RI'MOM}(\mu) &= \exp\left\{\int^x dx' \frac{\gamma(x')}{\beta(x')}\right\} \\ &= x^{\bar{\gamma}_0}\left\{1 + (\bar{\gamma}_1 - \bar{\beta}_1\bar{\gamma}_0)x + \frac{1}{2}[(\bar{\gamma}_1 - \bar{\beta}_1\bar{\gamma}_0)^2 + \bar{\gamma}_2 \right. \\ &\quad \left. + \bar{\beta}_1^2\bar{\gamma}_0 - \bar{\beta}_1\bar{\gamma}_1 - \bar{\beta}_2\bar{\gamma}_0]x^2 + \mathcal{O}(x^3)\right\}. \end{aligned} \tag{33}$$

TABLE III. Values of $Z_q$, $Z_S$, $Z_P$, $Z_V$, $Z_A$ and $Z_P/Z_S$ for all $N_f = 4$ ensembles analyzed.

| | $\beta = 2.10$–$32^3 \times 64$ | | | $\beta = 1.95$–$24^3 \times 48$ | | | $\beta = 1.90$–$24^3 \times 48$ | |
|---|---|---|---|---|---|---|---|---|
| | 3mp | 4mp | 5mp | 2mp | 3mp | 8mp | 1mp | 4mp |
| $Z_q^{\text{pert}}$ ($\mu_R = a^{-1}$) | 0.797(3) | 0.785(3) | 0.787(3) | 0.763(2) | 0.762(3) | 0.772(7) | 0.752(3) | 0.751(3) |
| $Z_S$ ($\mu_R = a^{-1}$) | 0.658(3) | 0.653(3) | 0.657(3) | 0.598(3) | 0.603(3) | 0.601(4) | 0.582(3) | 0.570(3) |
| $Z_P$ ($\mu_R = a^{-1}$) | 0.472(2) | 0.472(2) | 0.473(2) | 0.386(2) | 0.383(3) | 0.380(3) | 0.347(4) | 0.343(2) |
| $Z_V$ | 0.688(5) | 0.685(2) | 0.688(1) | 0.641(2) | 0.636(2) | 0.644(7) | 0.625(3) | 0.619(3) |
| $Z_A$ | 0.761(4) | 0.753(2) | 0.756(1) | 0.727(2) | 0.725(2) | 0.733(6) | 0.721(2) | 0.713(2) |
| $Z_P(I=1)/Z_S(I=1)$ | 0.717(3) | 0.724(3) | 0.720(3) | 0.645(5) | 0.634(5) | 0.632(5) | 0.597(7) | 0.602(5) |

TABLE IV. Dependence of local RCs on a lattice spacing variation, for the ensemble $2mp$.

| $a$[fm] | 0.072 | 0.078 | 0.084 |
|---|---|---|---|
| $Z_q^{\text{pert}}$ ($\mu_R = 10$ GeV) | 0.785(2) | 0.786(2) | 0.788(3) |
| $g^2\langle A^2\rangle$[GeV]$^2$ | 2.42(10) | 2.54(10) | 2.67(10) |
| $Z_S$ ($\mu_R = 10$ GeV) | 0.840(5) | 0.859(5) | 0.879(5) |
| $Z_P$ ($\mu_R = 10$ GeV) | 0.542(3) | 0.554(3) | 0.567(3) |
| $Z_P(I=1)/Z_S(I=1)$ | 0.645(5) | 0.645(5) | 0.645(5) |

As for the local RCs, we have added artifacts to the standard running formula, and we fit the coefficients $c_{a2p2}$ and $c_{p2m1}$. The anomalous dimension for $O_{44}$ is taken from Ref. [36] and reminded here for completeness

$$\gamma_{O_{44}} = \frac{32}{9}a - \frac{4}{243}[378N_f - 6005]a^2 + \frac{8}{6561}[10998N_f^2 - 6318\zeta(3)N_f - 467148N_f - 524313\zeta(3) + 3691019]a^3 + \mathcal{O}(a^4), \quad (34)$$

with $a = \frac{g^2}{16\pi^2}$.

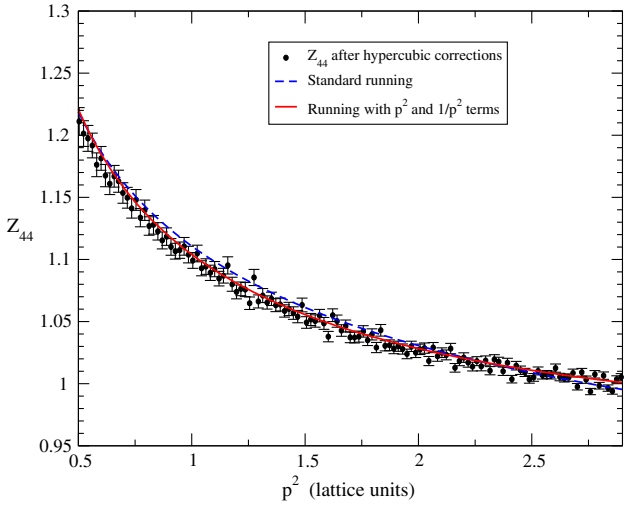


FIG. 11 (color online). Running of $Z_{44}$ for ensemble $3mp$, $\beta = 2.10$, $\mu = 0.0046$, $L = 32$, $T = 64$. The black points are the data after hypercubic artifacts removal. The dashed blue curve is the standard running expression Eq. (32), and the solid red line includes $1/(p^2_{\text{latt}})$ and $p^2_{\text{latt}}$ artifacts.

As can be seen in Fig. 11, only small lattice artifacts are affecting $Z_{44}$, compared to the case of local RCs. When adding $a^2p^2$ and $1/(a^2p^2)$ artifacts to the standard running expression Eq. (32), the $\chi^2$ of the fit is decreased and the $Z_{44}$ value changed by 3%–5%.

The results are sensitive to the values of the lattice spacing $a$ and of $\Lambda_{\text{QCD}}$ at the percent level and the uncertainties on both $a$ and $\Lambda_{\text{QCD}}$ will be taken into account in the analysis of systematic errors (see Sec. VIII).

## VI. CHIRAL EXTRAPOLATION AND LATTICE SPACING DEPENDENCE

To get the final values of RCs at each $\beta$ value, we need to perform the chiral extrapolation. The pion masses are way above the domain of validity of chiral perturbation theory (see Table II). This could not be avoided for technical reasons, namely simulation instabilities at low quark masses for $N_f = 4$ twisted-mass fermions. No theory tells us the expected behavior in terms of $m_\pi$. Notwithstanding this, some extended prejudice exists about the fact that the $m_\pi$ dependence is small. Indeed, left-hand side of Fig. 12 displays the pion mass dependence of local RCs for the three $\beta$ values under study and, as can be seen, all renormalization constants only depend very weakly on the pion mass, at least within the range where our pion masses lie. We thus perform a constant fit to get the chiral limit (dashed lines), in the assumption that the weak dependence we find still works for low pion masses. Though supported by the data of the local RCs shown here, this however remains an assumption and the systematic errors from our extrapolation at zero quark mass are poorly controlled. Further results closer to that limit would be helpful to clarify the situation.

Also visible on Fig. 12 is the fact that, if RCs are constant with respect to the pion mass, they are, to various extent and with the noticeable exception of $Z_S$, dependent on $\beta$. This is particularly striking on $Z_P, Z_V$ and $Z_A$, and to a lesser extent on $Z_q$. To analyze further this variation, we plot in Fig. 12 (rhs), RCs in the chiral limit versus the lattice spacing squared in logarithmic

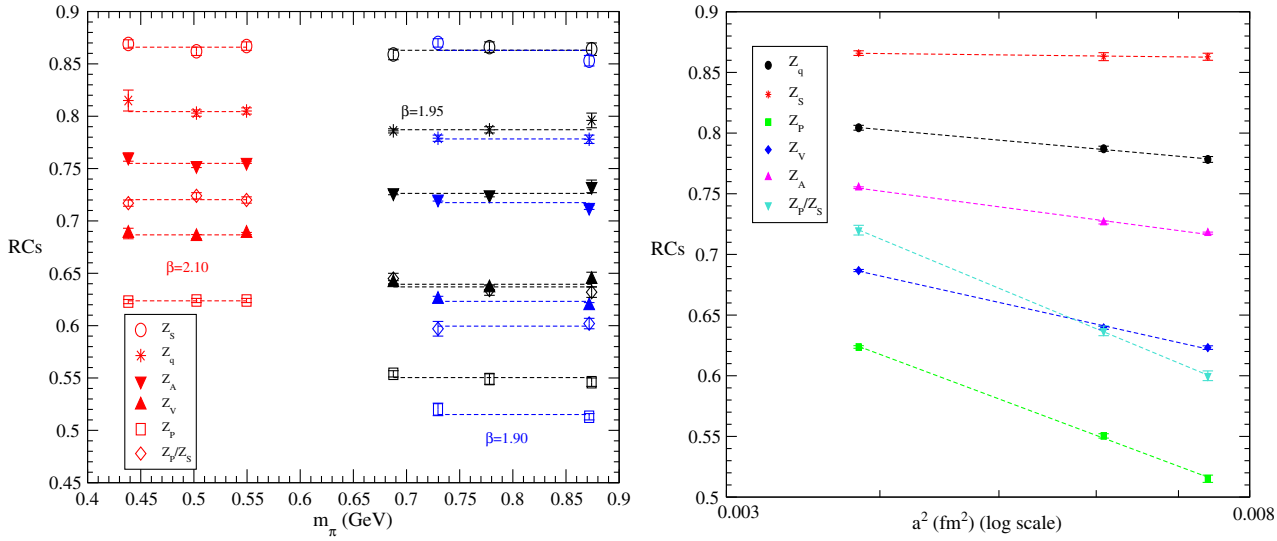


FIG. 12 (color online). lhs: $N_f = 4$ local RCs dependence with the pion mass. All RCs are given in the RI'-MOM scheme at 10 GeV. The straight dashed lines are constant fits for each $\beta$ values. The red points correspond to $\beta = 2.10$, the black ones to $\beta = 1.95$, and the blue ones to $\beta = 1.90$. rhs: local RCs after chiral extrapolation, versus $\log a^2$. All RCs follow a linear dependence with $\log a^2$ to a very high accuracy.

scale. All RCs follow with a very high accuracy a $\log(a^2)$ variation. Although, since RCs are used in practice to renormalize matrix elements computed at a fixed $\beta$ value, it is not crucial to take this dependence into account in the analysis, and it is still interesting to notice that the remaining lattice spacing dependence is in $\log(a^2)$.

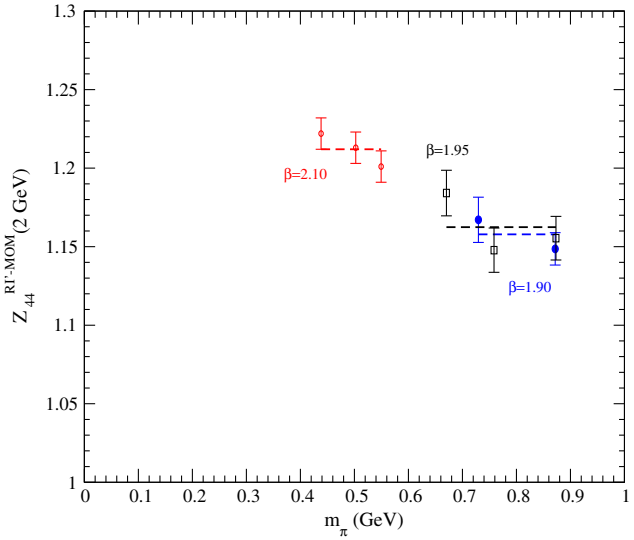


FIG. 13 (color online). lhs: $N_f = 4Z_{44}$ dependence with the pion mass. $Z_{44}$ is given in the RI'-MOM scheme at 2 GeV. The straight dashed lines are constant fits for each $\beta$ values. The red points correspond to $\beta = 2.10$, the black ones to $\beta = 1.95$, and the blue ones to $\beta = 1.90$.

Unlike local RCs, $Z_{44}$ exhibits a non-negligible pion mass dependence, as shown on Fig. 13. The values of $Z_{44}$ change by several percents (3%–4%) in the pion mass range considered (440–870 MeV), yet this change is mainly observed at $\beta = 1.95$. For this reason we perform the chiral extrapolation by a constant fit.

The pion mass dependence of $Z_{44}$ will be taken into account in evaluation of the systematics.

## VII. CONVERSION TO THE $\overline{\text{MS}}$ SCHEME AND EVOLUTION TO A REFERENCE SCALE

In order to make the connection with phenomenological calculations and experiments, which almost exclusively refer to the $\overline{\text{MS}}$ scheme, we convert our renormalization factors from RI'-MOM to $\overline{\text{MS}}$ using 3-loop perturbative conversion factors obtained from Ref. [19]. These latter are defined as $Z_q^{\overline{\text{MS}}} = C_q^{-1} Z_q^{RI'-MOM}$ and $Z_{\mathcal{O}}^{\overline{\text{MS}}} = C_{\mathcal{O}}^{-1} Z_{\mathcal{O}}^{RI'-MOM}$. In terms of the $\bar{\text{M}}\text{S}$ coupling constant $\alpha_{\overline{\text{MS}}} = \frac{g^2}{16\pi^2}$, and in the Landau gauge, these functions read[1]

[1]Setting the covariant gauge parameter $\lambda_{RI'}$ to zero leads to $\lambda_{\overline{\text{MS}}} = 0$ and since in addition $\alpha_{RI'} = \alpha_{\overline{\text{MS}}} + \mathcal{O}(\alpha_{\overline{\text{MS}}}^5)$ [19], these conversion functions have the same expression in the Landau gauge whether they are expressed in terms of $\overline{\text{MS}}$ or RI'-MOM variables.

$$C_q = 1 + [5C_F - (82 - 24\zeta(3))C_A + 28T_F N_f]\frac{C_F\alpha^2}{8} + [(678024\zeta(3) + 22356\zeta(4) - 213840\zeta(5) - 1274056)C_A^2 - (228096\zeta(3) + 31104\zeta(4) - 103680\zeta(5) - 215352)C_A C_F + 31536C_F^2 - (89856\zeta(3) - 760768)C_A T_F N_f + (68256 - 82944\zeta(3))C_F T_F N_f - 100480T_F^2 N_f^2]\frac{C_F\alpha^3}{5184} + \mathcal{O}(\alpha^4), \quad (35)$$

$$C_{S,P} = 1 - 4C_F\alpha + [(57 - 288\zeta(3))C_F + 332T_F N_f + (432\zeta(3) - 1285)C_A]\frac{C_F\alpha^2}{24} + [(-2493504\zeta(3) + 155520\zeta(5) + 2028348)C_A C_F - (-3368844\zeta(3) + 466560\zeta(5) + 6720046)C_A^2 + (-532224\zeta(3) + 186624\zeta(4) + 3052384)C_A T_F N_f + (-331776\zeta(3) - 186624\zeta(4) + 958176)C_F T_F N_f - (-451008\zeta(3) - 933120\zeta(5) + 2091096)C_F^2 - (27648\zeta(3) + 240448)T_F^2 N_f^2]\frac{C_F\alpha^3}{7776}, \quad (36)$$

$$C_{A,V} = 1 + \mathcal{O}(\alpha^4), \quad (37)$$

$$C_{44} = 1 + 31\frac{C_F\alpha}{9} + [(-1782\zeta(3) + 6404)C_A + (1296\zeta(3) - 228)C_F - 2668T_F N_f]\frac{C_F\alpha^2}{162} + [(-11944044\zeta(3) + 746496\zeta(4) + 524880\zeta(5) + 38226589)C_A^2 + (-4914432\zeta(3) - 2239488\zeta(4) + 8864640\zeta(5) + 3993332)C_A C_F + (369792\zeta(3) - 1492992\zeta(4) - 24752896)C_A T_F N_f + (10737792\zeta(3) + 1492992\zeta(4) - 9331200\zeta(5) - 3848760)C_F^2 - (-3234816\zeta(3) - 1492992\zeta(4) + 9980032)C_F T_F N_f + (221184\zeta(3) + 3391744)T_F^2 N_f^2]\frac{C_F\alpha^3}{69984} + O(a^4), \quad (38)$$

where $\zeta(n)$ is the Riemann zeta function and for the SU(3) color group, $T_F = \frac{1}{2}$, $C_F = \frac{4}{3}$, $C_A = 3$.

Using these expressions to convert our RI'-MOM results at a reference scale of 2 GeV to $\overline{\text{MS}}$ values also at 2 GeV leads to the final RCs listed in Table V.

To estimate the effect of the truncation in the perturbative series, we have also converted our results to $\overline{\text{MS}}$ at 2 GeV, but starting from RI'-MOM results at 10 GeV, converting them to $\overline{\text{MS}}$ scheme at 10 GeV, and then evolving the $\overline{\text{MS}}$ RCs from 10 to 2 GeV using the scale dependence predicted by the renormalization group equation [13]

$$R_{\mathcal{O}(\mu,\mu_0)} \coloneqq \frac{Z_{\mathcal{O}(\mu)}}{Z_{\mathcal{O}(\mu_0)}} = \exp\left\{-\int_{\bar{g}(\mu_0^2)}^{\bar{g}(\mu^2)} dg\frac{\gamma(g)}{\beta(g)}\right\}. \quad (39)$$

The effect is negligible on $Z_q$ (affecting only the last digit); it is of the order of 3.5% for $Z_S$, 4% for $Z_P$ and 2% for $Z_{44}$. For a perturbative series, the effect of truncation is relatively small, but compared with the systematic errors, it is far from being negligible.

## VIII. ESTIMATION OF THE SYSTEMATICS

The statistical uncertainties affecting the final results are rather small. Typically of the order of 1% for $Z_{44}$, and down to 2–5 per mille for local RCs. However, the analysis procedure leading to the final values of these RCs is quite complex and involves many nontrivial steps and systematic errors turn out to be dominant compared to the tiny statistical ones. A very careful study of systematics is thus

TABLE V. Local $N_f = 4$ RCs in the $\overline{\text{MS}}$ scheme at 2 GeV.

| $\beta$ | $Z_q$ | $Z_S$ | $Z_P$ | $Z_V$ | $Z_A$ | $Z_P/Z_S$ | $Z_{44}$ |
|---|---|---|---|---|---|---|---|
| 1.90 | 0.761(3) | 0.723(3) | 0.434(3) | 0.622(2) | 0.717(1) | 0.600(4) | 0.973(9) |
| 1.95 | 0.772(2) | 0.724(4) | 0.462(2) | 0.640(2) | 0.728(2) | 0.637(4) | 0.977(12) |
| 2.10 | 0.789(2) | 0.727(2) | 0.523(1) | 0.687(1) | 0.757(1) | 0.720(4) | 1.019(8) |

TABLE VI. Final results for $N_f = 4$ local RCs in the $\overline{\text{MS}}$ scheme at 2 GeV, for each $\beta$ values considered. The first parenthesis gives the statistical uncertainty, the second one the systematics due to the hypercubic removal procedure, combined with the running fit range, and the last number indicates the systematics due to the chiral extrapolation.

| $\beta$ | $Z_q$ | $Z_S$ | $Z_P$ | $Z_V$ | $Z_A$ | $Z_P/Z_S$ | $Z_{44}$ |
|---|---|---|---|---|---|---|---|
| 1.90 | 0.761(3)(5)(3) | 0.723(3)(5)(9) | 0.434(3)(3)(6) | 0.622(2)(1)(5) | 0.717(1)(2)(6) | 0.600(4)(4)(3) | 0.973(9)(7)(30) |
| 1.95 | 0.772(2)(6)(6) | 0.724(4)(5)(3) | 0.462(2)(4)(7) | 0.640(2)(1)(5) | 0.728(2)(2)(4) | 0.637(4)(4)(6) | 0.977(12)(11)(30) |
| 2.10 | 0.789(2)(6)(7) | 0.727(2)(5)(4) | 0.523(1)(4)(1) | 0.687(1) (1)(2) | 0.757(1)(2)(4) | 0.720(4)(2)(5) | 1.019(8)(6)(30) |

unavoidable to produce *in fine* reliable and meaningful results.

Sources of systematic uncertainties are manifold. They arise from the removal of hypercubic corrections, from the running fit, from the chiral extrapolation, and from the uncertainties on the lattice spacing and on $\Lambda_{\text{QCD}}$. We have carefully estimated each source of uncertainties and final results are given in Table VI. The first parenthesis gives the statistical uncertainty. The second one comes from the systematics due to the hypercubic removal procedure, combined with the running fit range. We have varied both the range of $p^2$ used in the hypercubic removal procedure and in the running fit, separately, to estimate the maximal variation on the final RCs value. This leads to the systematics indicated in the second parenthesis. Finally, the last number indicates the systematics due to the chiral extrapolation.

The uncertainties on the lattice spacing $a$ and on the value of $\Lambda_{\text{QCD}}$ have also been propagated to the RCs and included in the errors quoted in Table VI. We have varied $a$ by $\pm 5\%$ from its central value and taken $\Lambda_{\text{QCD}} = 316(13)$ MeV from Ref. [28].

Systematics are estimated separately on local and on twist-2 renormalization constants. They indeed behave quite differently, whether it concerns their pion mass dependence, or their sensitivity to lattice spacing and $\Lambda_{\text{QCD}}$. The hypercubic corrections and the running lead to an uncertainty which does not exceed 1%. The pion mass dependence of all local RCs is weak and the uncertainties associated with the chiral extrapolation small.

The uncertainty on the lattice spacing and on $\Lambda_{\text{QCD}}$, propagated to the local RCs, gives a very small sensitivity for $Z_q$ and $\frac{Z_P}{Z_S}$, and an effect of about 2% for $Z_S, Z_P$ (see Table IV for example). In particular, the very effect of the uncertainty in the lattice spacing is $\sim 0.001$ for $Z_q$, $Z_S$ and $Z_P$, and can be neglected for $Z_V$, $Z_A$ or $Z_P/Z_S$ that do not run with momenta in perturbation.

The situation is a bit different for $Z_{44}$. Uncertainties due to the $H(4)$ corrections and the running fit are of the order of the statistical errors, the dominant source of uncertainties comes clearly from the chiral extrapolation, which induces errors of the order of 3%. In addition, the errors on $a$ and $\Lambda_{\text{QCD}}$ produce an additional uncertainty on $Z_{44}$ of the order of 3%.

Finally we have compared our results with the values for local RCs given in Ref. [8]. These latter have been obtained using the "democratic" selection of momenta. Restricting our fitting interval to the one used in this reference ("method M1") we find close results, a precise comparison being however difficult since only statistical errors are reported in [8]. In addition, taking into account statistical and systematic errors, our results are also compatible with those from [17] for $Z_{44}$.

## IX. CONCLUSION

We have presented an original analysis of quark propagator, vertex functions and twist-2 operators renormalization constants for $N_f = 4$ twisted-mass fermions. We have implemented a systematic and rigorous procedure to correct for hypercubic lattice artifacts. This nonperturbative method, avoiding the selection of momenta usually done in this kind of analysis and the use of perturbative formulas, allows us to take advantage of all the data and to check the running over a wide range of momenta. We have applied our analysis procedure not only to local operators, but also to the twist-2 operator $O_{44}$. $\mathcal{O}(a^2)$ lattice artifacts have also been efficiently subtracted. In order to compare with experimental values obtained for the corresponding matrix elements, all our results, obtained in the RI'-MOM scheme, have been converted to the $\overline{\text{MS}}$ scheme at 2 GeV. A precise estimate of systematic errors have also been performed and these latter are shown to be dominant in the case of twist-2 operator $O_{44}$. Concerns could be raised because of the fact that the RI-MOM scheme requires gauge fixing. There could in principle be fluctuations arising from the Gribov ambiguity. However, several studies explored this idea in the 1990s [37–40] as well as later on with Ginsparg-Wilson fermions [26] and have shown that this effect is less than 1% and thus the dependence on gauge fixing is negligible. Of course one has to mention that all this previous work was in the quenched approximation.

The method developed here will be applied in the near future to the new gauge configurations, at the physical pion mass, generated by the ETM Collaboration.

## ACKNOWLEDGMENTS

We thank P. Boucaud, F. de Soto, X. Du, Z. Liu, K. Petrov and particularly A. Vladikas for useful discussions. We are also grateful to N. Carrasco, P. Dimopoulos, R. Frezzotti, V. Lubicz and S. Simula for their careful reading of the manuscript and their remarks. This work was granted

access to the HPC resources of CINES and IDRIS under the allocations 2013-052271 and 2014-052271 made by GENCI. Propagator computations have also extensively used CINECA GPUs in the framework of the DECI-9 project DEC09-NPR-LQCD. Most of the analysis has been done in Lyon-CCIN2P3, thanks to the massive storage and large CPU resources provided. We are grateful to the staff members of all these computing centers for their constant help. This work was supported by the CNRS and the Alexander von Humboldt Foundation (S. Z.).

[1] G. Martinelli, C. Pittori, C. T. Sachrajda, M. Testa, and A. Vladikas, A general method for nonperturbative renormalization of lattice operators, Nucl. Phys. **B445**, 81 (1995).

[2] D. Becirevic, P. Boucaud, J. P. Leroy, J. Micheli, O. Pene, J. Rodriguez-Quintero, and C. Roiesnel, Asymptotic behavior of the gluon propagator from lattice QCD, Phys. Rev. D **60**, 094509 (1999); Asymptotic scaling of the gluon propagator on the lattice, Phys. Rev. D **61**, 114508 (2000).

[3] P. Boucaud, F. de Soto, J. P. Leroy, A. Le Yaouanc, J. Micheli, H. Moutarde, O. Pene, and J. Rodriguez-Quintero, Quark propagator and vertex: Systematic corrections of hypercubic artifacts from lattice simulations, Phys. Lett. B **575**, 256 (2003).

[4] F. de Soto and C. Roiesnel, On the reduction of hypercubic lattice artifacts, J. High Energy Phys. 09 (2007) 007.

[5] P. Boucaud, A. Le Yaouanc, J. P. Leroy, J. Micheli, O. Pene, and J. Rodriguez-Quintero, Testing Landau gauge OPE on the lattice with a condensate, Phys. Rev. D **63**, 114003 (2001); Consistent OPE description of gluon two point and three point Green function?, Phys. Lett. B **493**, 315 (2000).

[6] M. Lavelle and M. Oleszczuk, The operator product expansion of the QCD propagators, Mod. Phys. Lett. A **07**, 3617 (1992); J. Ahlbach, M. Lavelle, M. Schaden, and A. Streibl, Propagators and four-dimensional condensates in pure QCD, Phys. Lett. B **275**, 124 (1992); D. Dudal, H. Verschelde, R. E. Browne, and J. A. Gracey, A determination of $\langle A_\mu^2 \rangle$ and the nonperturbative vacuum energy of Yang-Mills theory in the Landau gauge, Phys. Lett. B **562**, 87 (2003); D. Dudal, O. Oliveira, and N. Vandersickel, Indirect lattice evidence for the refined Gribov-Zwanziger formalism and the gluon condensate $\langle A^2 \rangle$ in the Landau gauge, Phys. Rev. D **81**, 074505 (2010); K. I. Kondo, Vacuum condensate of mass dimension 2 as the origin of mass gap and quark confinement, Phys. Lett. B **514**, 335 (2001); E. Megias, E. R. Arriola, and L. L. Salcedo, Dimension two condensates and the Polyakov loop above the deconfinement phase transition, J. High Energy Phys. 01 (2006) 073; E. Ruiz Arriola, P. O. Bowman, and W. Broniowski, Landau-gauge condensates from the quark propagator on the lattice, Phys. Rev. D **70**, 097505 (2004).

[7] B. Blossier *et al.* (ETM Collaboration), Renormalization constants of quark bilinears in lattice QCD with four dynamical Wilson quarks, *Proc. Sci.*, LATTICE2011 (2011) 233 [arXiv:1112.1540].

[8] N. Carrasco *et al.* (The European Twisted Mass Collaboration), Up, down, strange and charm quark masses with $N_f = 2 + 1 + 1$ twisted mass lattice QCD, Nucl. Phys. **B887**, 19 (2014).

[9] P. Dimopoulos *et al.* (ETM Collaboration), Renormalization constants for Wilson fermion lattice QCD with four dynamical flavours, *Proc. Sci.*, LATTICE2010 (2010) 235 [arXiv:1101.1877].

[10] R. Frezzotti and G. C. Rossi, Chirally improving Wilson fermions. 1. O($a$) improvement, J. High Energy Phys. 08 (2004) 007; Twisted mass lattice QCD with mass nondegenerate quarks, Nucl. Phys. B, Proc. Suppl. **128**, 193 (2004) .

[11] B. Blossier, P. Boucaud, M. Brinet, F. De Soto, V. Mornas, O. Pène, K. Petrov, and J. Rodrguez-Quintero, Novel method for the physical scale setting on the lattice and its application to $N_f = 4$ simulations, Phys. Rev. D **89**, 034026 (2014).

[12] A. Vladikas, in *Modern Perspectives in Lattice QCD: Quantum Field Theory and High Performance Computing, Lecture Notes delivered at the XCIII Les Houches Summer School (2009)* (Oxford University Press, New York, 2011).

[13] M. Gockeler, R. Horsley, H. Oelrich, H. Perlt, D. Petters, P. E. L. Rakow, A. Schafer, G. Schierholz, and A. Schiller, Nonperturbative renormalization of composite operators in lattice QCD, Nucl. Phys. **B544**, 699 (1999).

[14] C. Alexandrou, M. Constantinou, T. Korzec, H. Panagopoulos, and F. Stylianou, Renormalization constants of local operators for Wilson type improved fermions, Phys. Rev. D **86**, 014505 (2012).

[15] M. Constantinou *et al.* (ETM Collaboration), Nonperturbative renormalization of quark bilinear operators with $N_f = 2$ (tmQCD) Wilson fermions and the tree-level improved gauge action, J. High Energy Phys. 08 (2010) 068.

[16] B. Blossier, P. Boucaud, M. Brinet, F. De Soto, Z. Liu, V. Morenas, O. Pene, K. Petrov, and J. Rodríguez-Quintero, Renormalization of quark propagators from twisted-mass lattice QCD at $N_f = 2$, Phys. Rev. D **83**, 074506 (2011).

[17] C. Alexandrou, M. Constantinou, S. Dinter, V. Drach, K. Jansen, C. Kallidonis, and G. Koutsou Nucleon form factors and moments of generalized parton distributions using $N_f = 2 + 1 + 1$ twisted mass fermions, Phys. Rev. D **88**, 014509 (2013).

[18] J. W. Negele, Understanding parton distributions from lattice QCD: Present limitations and future promise, Nucl. Phys. **A711**, 281 (2002).

[19] J. A. Gracey, Three loop anomalous dimension of nonsinglet quark currents in the RI-prime scheme, Nucl. Phys. **B662**, 247 (2003).

[20] B. Blossier, Ph. Boucaud, M. Brinet, F. De Soto, V. Morenas, O. Pène, K. Petrov, and J. Rodríguez-Quintero (ETM Collaboration), High statistics determination of the

strong coupling constant in Taylor scheme and its OPE Wilson coefficient from lattice QCD with a dynamical charm, Phys. Rev. D **89**, 014507 (2014).

[21] B. Blossier, P. Boucaud, M. Brinet, F. De Soto, X. Du, V. Morenas, O. Pene, K. Petrov, and J. Rodriguez-Quintero, Strong Running Coupling at $\tau$ and $Z_0$ Mass Scales from Lattice QCD, Phys. Rev. Lett. **108**, 262002 (2012).

[22] Petros Dimopoulos, in Paris ETMC meeting, May 2012 (unpublished).

[23] J.-R. Cudell, A. Le Yaouanc, and C. Pittori, Pseudoscalar vertex, Goldstone boson and quark masses on the lattice, Phys. Lett. B **454**, 105 (1999).

[24] P. Dimopoulos, R. Frezzotti, C. Michael, G. C. Rossi, and C. Urbach, O($a^2$) cutoff effects in lattice Wilson fermion simulations, Phys. Rev. D **81**, 034509 (2010).

[25] H. Pagels, Dynamical chiral symmetry breaking in quantum chromodynamics, Phys. Rev. D **19**, 3080 (1979).

[26] C. Gattringer, M. Gockeler, P. Huber, and C. B. Lang, Renormalization of bilinear quark operators for the chirally improved lattice Dirac operator, Nucl. Phys. **B694**, 170 (2004).

[27] B. Blossier, P. Boucaud, M. Brinet, F. De Soto, V. Morenas, O. Pene, K. Petrov, and J. Rodriguez-Quintero, Testing the OPE Wilson coefficient for $A^2$ from lattice QCD with a dynamical charm, Phys. Rev. D **87**, 074033 (2013).

[28] B. Blossier, Ph. Boucaud, M. Brinet, F. De Soto, X. Du, M. Gravina, V. Morenas, O. Pene, K. Petrov, and J. Rodriguez-Quintero, Ghost-gluon coupling, power corrections, and $\Lambda_{\overline{\rm MS}}$ from lattice QCD with a dynamical charm, Phys. Rev. D **85**, 034503 (2012).

[29] B. Blossier, Ph. Boucaud, F. De Soto, V. Morenas, M. Gravina, O. Pène, and J. Rodríguez-Quintero (ETM Collaboration), Ghost-gluon coupling, power corrections and $\Lambda_{\overline{\rm MS}}$ from twisted-mass lattice QCD at $N_f = 2$, Phys. Rev. D **82**, 034510 (2010).

[30] P. Boucaud, F. De Soto, J. P. Leroy, A. Le Yaouanc, J. Micheli, O. Pene, and J. Rodriguez-Quintero, Ghost-gluon running coupling, power corrections and the determination of $\Lambda_{\overline{\rm MS}}$, Phys. Rev. D **79**, 014508 (2009).

[31] P. Boucaud, J. P. Leroy, A. Le Yaouanc, A. Y. Lokhov, J. Micheli, O. Pene, J. Rodriguez-Quintero, and C. Roiesnel, Non-perturbative power corrections to ghost and gluon propagators, J. High Energy Phys. 01 (2006) 037.

[32] A. Ayala, A. Bashir, D. Binosi, M. Cristoforetti, and J. Rodriguez-Quintero, Quark flavor effects on gluon and ghost propagators, Phys. Rev. D **86**, 074512 (2012).

[33] P. Boucaud, F. de Soto, J. P. Leroy, A. Le Yaouanc, J. Micheli, H. Moutarde, O. Pene, and J. Rodriguez-Quintero, Artifacts and $\langle A^2 \rangle$ power corrections: Reexamining $Z_\psi(p^2)$ and $Z_V$ in the momentum-subtraction scheme, Phys. Rev. D **74**, 034505 (2006).

[34] K. G. Chetyrkin and A. Retey, Renormalization and running of quark mass and field in the regularization invariant and $\overline{\rm MS}$ schemes at three loops and four loops, Nucl. Phys. **B583**, 3 (2000).

[35] T. van Ritbergen, J. A. M. Vermaseren, and S. A. Larin, The four loop beta function in quantum chromodynamics, Phys. Lett. B **400**, 379 (1997); J. A. M. Vermaseren, S. A. Larin, and T. van Ritbergen, The four loop quark mass anomalous dimension and the invariant quark mass, Phys. Lett. B **405**, 327 (1997); K. G. Chetyrkin, Quark mass anomalous dimension to $\mathcal{O}(\alpha_s^4)$, Phys. Lett. B **404**, 161 (1997).

[36] J. A. Gracey, Three loop anomalous dimension of the second moment of the transversity operator in the $\overline{\rm MS}$ and RI' schemes, Nucl. Phys. **B667**, 242 (2003).

[37] M. L. Paciello, S. Petrarca, B. Taglienti, and A. Vladikas, Gribov noise of the lattice axial current renormalization constant, Phys. Lett. B **341**, 187 (1994).

[38] M. L. Paciello, C. Parrinello, S. Petrarca, B. Taglienti, and A. Vladikas, Gribov copies and smeared correlation functions in lattice QCD, Phys. Lett. B **289**, 405 (1992).

[39] C. Parrinello, S. Petrarca, and A. Vladikas, A preliminary study of the Gribov ambiguity in lattice SU(3) Coulomb gauge, Phys. Lett. B **268**, 236 (1991).

[40] M. L. Paciello, C. Parrinello, S. Petrarca, B. Taglienti, and A. Vladikas, SU(3) lattice gauge fixing with overrelaxation and Gribov copies, Phys. Lett. B **276**, 163 (1992); Erratum: SU(3) lattice gauge fixing with overrelaxation and Gribov copies, Phys Lett. B **281**, 417(E) (1992).